Journal of Petroleum Science and Engineering 212 (2022) 110247

Contents lists available at ScienceDirect

Journal of Petroleum Science and Engineering

journal homepage: www.elsevier.com/locate/petrol

Insights into the mechanical stratigraphy and vertical fracture patterns in tight oil sandstones: The Upper Triassic Yanchang Formation in the eastern Ordos Basin, China

Wenya Lyu [a,b], Lianbo Zeng [a,b,*], Peng Lyu [b,c], Tao Yi [d], Shaoqun Dong [a,b,e], Shengjiao Wang [b], Xiang Xu [b], Huan Chen [b]

[a] State Key Laboratory of Petroleum Resources and Prospecting, China University of Petroleum, Beijing, 102249, PR China
[b] College of Geosciences, China University of Petroleum, Beijing, 102249, PR China
[c] Exploration and Development Research Institute of Sinopec Shanghai Offshore Oil & Gas Company, Shanghai, 200120, PR China
[d] No.12 Oil Production Plant of Petro China Changqing Oilfield Company, Qingyang, 710018, PR China
[e] College of Sciences, China University of Petroleum, Beijing, 102249, PR China

ARTICLE INFO

Keywords:
Natural fractures
Mechanical stratigraphy
Tight oil sandstone
Fracture hierarchy
Fracture pattern
Yanchang formation
Ordos basin

ABSTRACT

Vertical fracture patterns are mapped in the outcrops to analyze the impact of mechanical stratigraphy on vertical fractures in the relatively undeformed Upper Triassic tight oil sandstones of the Yanchang Formation along Yanhe River in the east Ordos Basin, China. The relationship between natural fractures and different bounding interfaces are analyzed based on rock relative strength measurement by N-type Schmidt Hammer, fracture and facies description in the outcrops. According to the probability of the bounding interface terminating natural fractures being more than 20%, seven types of mechanical interfaces terminating fracture longitudinal propagation are identified, namely 1) the interface of laminae-set or laminae co-sets, 2) bedding surface interface, 3) accretionary interface, 4) mudstone interbed, 5) mudstone barrier, 6) calcareous barrier and 7) depositional scour interface. According to fracture sizes and the mechanical interfaces which constrain fracture propagation, the vertical fractures are divided into micro-scale, small-scale, meso-scale and macro-scale ones. Three possible vertical fracture patterns in various sedimentary microfacies of the shallow water delta deposits are discussed based on field outcrop observation, the restriction capacities of different mechanical interfaces and the temporally changing tectonic stress. Finally, the application of vertical fracture patterns for subsurface fracture prediction is carried out in the Ansai Oilfield in the eastern Ordos Basin, China. The predicted fractures in wells are consistent with the fractures obtained from cores and conventional logs. This study links sedimentary stratigraphy, mechanical stratigraphy and natural fractures in the tight oil sandstones within a relatively undeformed setting, meanwhile unravels the vertical fracture patterns in different sedimentary microfacies of the shallow water delta deposits in the study area. The results will thus guide subsurface fracture prediction between wells in the tight oil sandstones of the eastern Ordos Basin.

1. Introduction

Tight oil, accumulating in tight sandstones or carbonates, is an important and hot unconventional petroleum resource around the world (Zou et al., 2015; Eia, 2021). Fractures are important storage spaces and main fluid-flow pathways in tight oil sandstones with low matrix porosity and permeability (Zeng et al., 2013; Lyu et al., 2019). Therefore, the fluid flow prediction in tight oil sandstones requires understanding the fracture network distribution. Quantitative fracture parameters in single wells can be obtained from cores, image logs and thin sections (Lai et al., 2018; Lyu et al., 2019); however, the network of fractures, especially vertical fractures, are poorly sampled by vertical borehole data (Nelson et al., 2000). The quantitative fracture parameters and patterns between wells are hard to be obtained by low-resolution seismic data and the relatively low-accuracy reservoir geomechanical method (Chen et al., 2016; Lyu et al., 2021).

Under the effect of a certain regional tectonic stress within a relatively undeformed setting, the fracture patterns are largely controlled by

* Corresponding author. College of Geoscience, China University of Petroleum, Beijing, 102249, PR China.
E-mail addresses: wylvwenwen@163.com (W. Lyu), lbzeng@sina.com (L. Zeng).

https://doi.org/10.1016/j.petrol.2022.110247
Received 25 August 2021; Received in revised form 20 December 2021; Accepted 29 January 2022
Available online 10 February 2022

mechanical stratigraphy rather than faults and folds (Underwood et al., 2003; Rustichelli et al., 2012). Mechanical stratigraphy refers to rock strata with similar mechanical behavior or consistent mechanical properties (Cooke et al., 2006; Laubach et al., 2009). Mechanical stratigraphy consists of the mechanical unit and mechanical interface (Cooke et al., 2006; Rustichelli et al., 2013, Fig. 1). The mechanical interface can be an interface or a layer with a certain thickness, which terminates fracture longitudinal propagation (Fig. 1). In general, fractures are developed in a mechanical unit and terminated at the mechanical interfaces (Cooke et al., 2006, Fig. 1). In other words, fracture stratigraphy is equal to mechanical stratigraphy during fracture formation. Thus, determining the mechanical interfaces and reasonably dividing the mechanical stratigraphy provide an important guidance for understanding and predicting fracture distribution between wells (McGinnis et al., 2017).

Many studies have been done on the impact of mechanical stratigraphy on fracture distribution, pattern, linkage and cluster formation, thus providing guidance for subsurface fracture prediction in aquifer and petroleum reservoirs (Underwood et al., 2003; Laubach et al., 2009; Lamarche et al., 2012; Panza et al., 2016; McGinnis et al., 2017; Dashti et al., 2018; Balsamo et al., 2020; Boersma et al., 2020). However, most of these researches were focused on carbonate reservoirs, chalks and mudstones, and few works have been done on tight sandstone reservoirs. In addition, some researchers discussed the controlling role of sedimentary facies or stratigraphic architecture on mechanical and fracture stratigraphy in carbonates, sandstones, etc (Barbier et al., 2012; Ogata et al., 2017; Cawood and Bond, 2018; Giuffrida et al., 2020). However, fracture patterns in different sedimentary faices have not been fully discussed. Additionally, the impact of mechanical stratigraphy on fracture pattern in tight sandstones needs further study since the characteristics of mechanical stratigraphy, sedimentary facies and fracture patterns in tight sandstones are different from those in carbonates, chalks and mudstones.

The original components and structures of rocks change due to the different hydrodynamic conditions, depositional environment and diagenetic modifications after deposition, and the rock mechanics properties of the internal layer are different, showing strong heterogeneity (Underwood et al., 2003; Larsen et al., 2010). Consequently, the sedimentary stratigraphy is not always in accordance with the mechanical stratigraphy (Larsen et al., 2010). Generally, a mechanical unit can be a single sedimentary unit or multiple sedimentary units with similar rock mechanical properties (Cooke et al., 2006). In addition, various type and degree of diagenetic modifications between layers with different grain size could result in temporally changing of mechanical stratigraphy (Shackleton et al., 2005; Cawood and Bond, 2018). The present-day mechanical properties in a fractured rock may not be the same as the properties when the fractures were formed (Panza et al., 2016). Alternatively, fractures may form in the early stages of burial diagenesis when the interfaces did not act as mechanical interfaces (Lamarche et al., 2012). Therefore, fracture stratigraphy is not necessarily equal to the present-day mechanical stratigraphy because of the time-dependent feature of rock mechanical properties (Laubach et al., 2009).

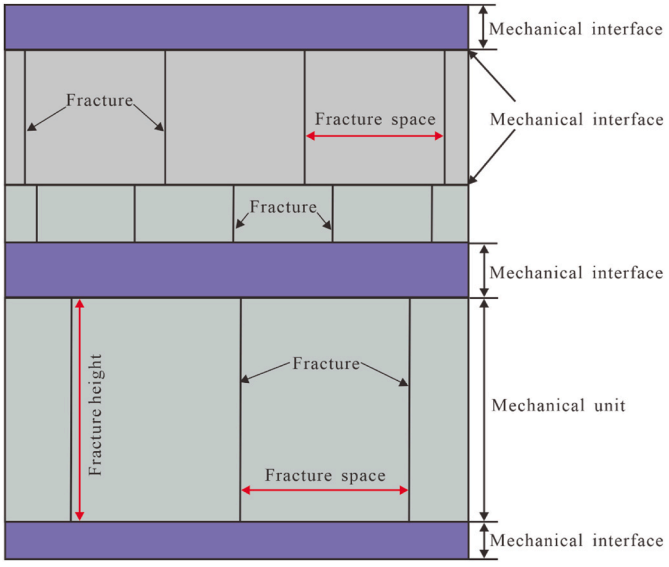

Fig. 1. The schematic diagram shows mechanical stratigraphy.

Vertical fractures are widely developed in the tight sandstones of the Upper Triassic Yanchang Formation in the Ordos Basin (Zeng and Li, 2009). The fracture characteristics, formation time, distribution characteristics, contributions to reservoir physical properties and oil production of the Upper Triassic Yanchang Formation have been studied (Zeng et al., 2007; Zeng and Li, 2009; Zhou et al., 2012; Wang et al., 2013; Ju et al., 2014; Lyu et al., 2019). Fractures are obviously controlled by the sedimentary bedding from the outcrops, since fractures are generally normal to and terminate at the sedimentary bedding surface (Zeng and Li, 2009). Fractures commonly have regular spaces in the same sedimentary layers; and the average spacing of intraformational fractures is present a positively linear correlation to the bed thickness (Lyu et al., 2019). However, sedimentary stratigraphy and mechanical stratigraphy are not in accordance in most cases (Larsen et al., 2010). The impact of mechanical stratigraphy on fracture patterns is not clear in the Ordos Basin.

In this study, firstly, rock relative strength measurement by N-type Schmidt Hammer, fracture and facies description are carried on the outcrops of the tight oil sandstones of the Yanchang Formation in the eastern Ordos Basin (Fig. 2). The relationships between natural fractures and different bonding interfaces in the studied outcrops are analyzed. Then, the effectiveness of different types of bounding interfaces as mechanical interfaces is assessed based on the probability of the bounding interface terminating natural fractures. Fracture hierarchy division is established based on the different mechanical interfaces, which constrain fracture propagation, and fracture sizes. Moreover, vertical fracture patterns in different sedimentary microfacies of the shallow water delta deposits are discussed based on the impact of mechanical stratigraphy. In addition, according to a total of 284.2 m of cores from 8 vertical wells, conventional logs from 123 wells and electrical borehole image logs from 2 wells, subsurface fracture identification and sedimentary study are conducted on the tight oil sandstones of Chang 6 in the Ansai Oilfled, Ordos Basin. Finally, the application of vertical fracture patterns for subsurface fracture prediction is carried out in Ansai Oilfield in the east Ordos Basin, China. The study describes the relationship among sedimentary stratigraphy, mechanical stratigraphy and natural fractures in the tight oil sandstones within a relatively undeformed setting. Simultaneously, it draws vertical fracture patterns from stratigraphic information, which provides guidance for subsurface fracture prediction between wells in the study area.

2. Geological setting

2.1. Location and structure

The Ordos Basin is located in central China (Fig. 3a). According to the modern tectonic features and basement characteristics of the Ordos Basin, it can be divided into six tectonic units, including the Jinxi fault-fold belt to the east, the Weibei uplift to the south, the Tianhuan depression and the Western thrust belt to the west, the Yimeng uplift to the north and the Yishan slope in the central (Lai et al., 2019, Fig. 3b).

The studied outcrops of the Upper Triassic Yanchang Formation are located in the east Yishan slope of the Ordos Basin, and well-exposed along Yanhe River in the Yanchang County, Yan'an City (Figs. 3b and c). According to the lithology, fossil assemblages, the Upper Triassic

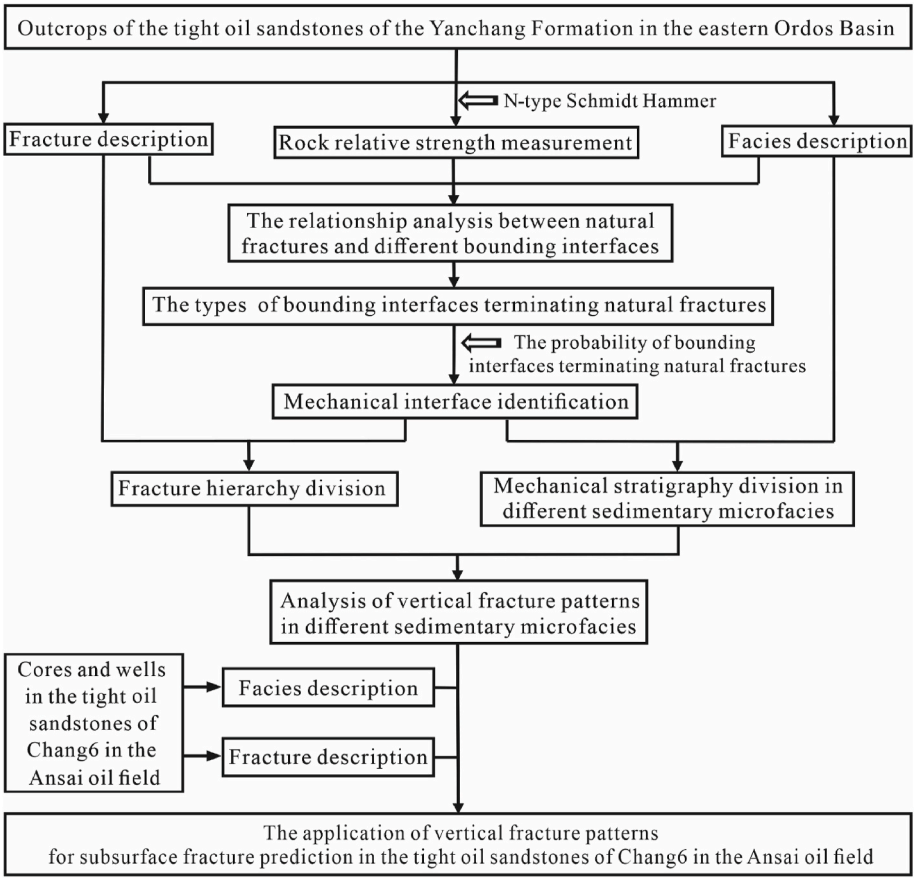

Fig. 2. The workflow of the research steps.

Yanchang Formation is divided into ten members (Chang 10 to Chang 1) from bottom to top. The outcrops of Chang 10 to Chang 2 run from the west bank of the Yellow River along the Yanhe River to the west via Wangjiahe Village, Zhangjiatan Town, Yanchang County to Ganguyi Town, Yan'an City (Fig. 3d). The outcrops of Chang 1 extend westward from Yaodian to Qiaogou Town, Yan'an, and are exposed along a road. The total length of the Yanchang Formation outcrops is about 60–80 km. The outcrops are about 20 m high along the road and 3 m high along the valley of Yanhe River. In addition, the studied outcrops are analog ones of the Yanchang Formation of Ansai oilfield, which is located in Ansai City (Fig. 3b).

Under the effect of the surrounding mountains (Qinling, Liupang, Huolan, Yin and Lyuliang Mountains), faults and folds are distributed along the margins of the Ordos Basin (Fig. 3b). Whereas, the Yishan slope is in a relative undeformed setting, and a smooth monocline with an east-west dip of less than 1° exits (Du et al., 2019; Xu and Wang, 2020). Based on the tectonic deformation traces and the regional tectonic deformation characteristics, the Upper Triassic Yanchang Formation has experienced four episodes of tectonic compression stresses, namely Late Triassic, Late Triassic to Late Cretaceous, Paleogene to Neogene and Present day (Yang, 2002). According to the longitudinal bending folds, conjugate fractures and shear zones in the Jurassic strata and Paleogene strata of the Ordos Basin, and the occurrence of the principal stress, the directions of SHmax of Late Triassic to Late Cretaceous and Paleogene to Neogene are 310° and 30°, respectively (Yang et al., 2008; Zeng, 2008). Based on rock acoustic emissions of the Yanchang Formation, the magnitudes of the SHmax of Late Triassic to Late Cretaceous and Paleogene to Neogene are 93 MPa and 87 MPa, respectively (Zhang, 1996).

2.2. Stratigraphy and sedimentology

The Ordos Basin is rich in oil and gas resources and mainly contains two hydrocarbon systems, that is Paleozoic gas system and Mesozoic oil system (Yang et al., 2013). Abundant oil resources of Mesozoic oil system are present in the Upper Triassic Yanchang Formation (Zhang et al., 2015). The Upper Triassic Yanchang Formation is overlain by Early Jurassic strata, and rests unconformably on the Middle Triassic Zhifang Formation (Fig. 4). The Upper Triassic Yanchang Formation of the study area is developed lacustrine-delta continental deposits and mainly controlled by the northeast sediment source (Lai et al., 2017; Qu et al., 2020). The Ordos Bain experienced three large subsidence during Early and Middle Triassic, and formed three large-scale lacustrine transgressions marked by shale developed in Chang 9, Chang 7 and Chang 4 + 5, respectively (Fig. 4; Zhao et al., 2015; Lai et al., 2016; Li et al., 2020). The delta deposits of the Yanchang Formation of the studied outcrops and Ansai Oilfield are mainly distributary channel, mouth bar, overbank sandbody, sheet sandbody and interdistributary bay (Fu, 2013).

The cumulative thickness of the Yanchang Formation in the studied outcrops is 1140.8 m (He et al., 2011). From bottom to top, the lithology of the Yanchang Formation consists of grayish-green medium-thick massive fine-grained sandstone, grey siltstone interbedded with dark-grey mudstone and black oil shale (Fig. 4). Some fine-grained sandstones and shales are rich in oil in the outcrops of Chang 6 to Chang 8, where oil seepage is present (He et al., 2004). Petrophysical parameter analysis shows that the porosity of the Yanchang Formation is mainly less than 10% and the average permeability is less than 1×10^{-3} μm^2 (1md) (He et al., 2004; Golsanami et al., 2021a).

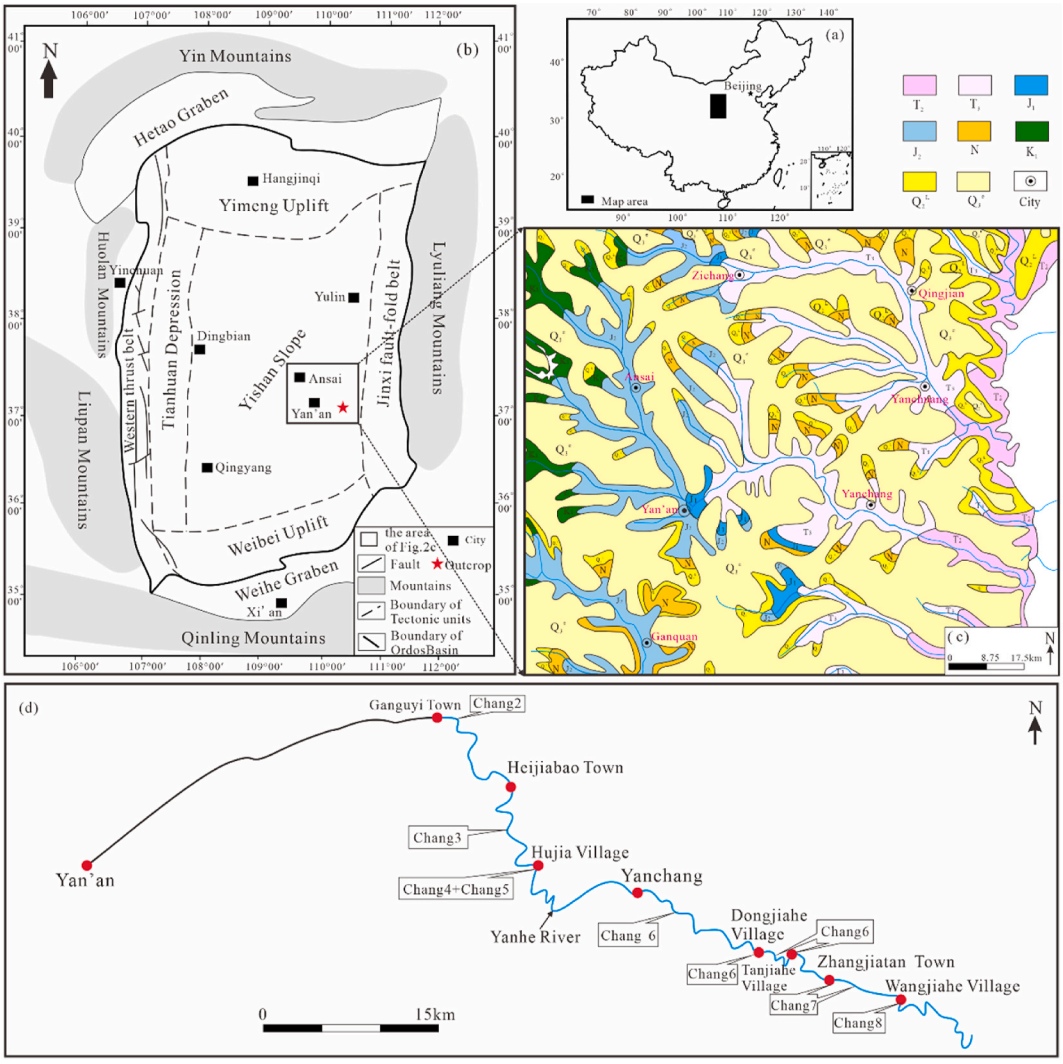

Fig. 3. Location map of the Ordos Basin and outcrops. (a) Location of the Ordos Basin. (b) Location of the studied outcrops, main cities and tectonic units of the Ordos Basin, with surface-exposed faults. (c) Geological map showing the studied outcrops in the eastern Ordos Basin. (d) Location of the studied outcrops along Yanhe River in the eastern Ordos Basin (Figs. 3a and b were modified from Zeng and Li, 2009; Lyu et al., 2016a, 2017, 2019.).

3. Methods

The outcrops of Chang 1 to Chang 10 were firstly surveyed to understand the overall features of the Yanchang Formation, and determine the boundary of each member of the Yanchang Formation. The detailed analysis, measurement and photograph of sedimentary facies, fractures and mechanical stratigraphies were predominantly carried on the outcrops of Chang 6 to Chang 8, where tight oil resources are mainly developed.

3.1. Facies description

Lithological characteristics in the outcrops were determined through petrographic analysis. The lithology profiles in wells of the tight sandstones of Chang 6 in Ansai Oilfield were determined by cores and conventional logs such as gamma ray log (GR), spontaneous potential log (SP) and the caliper log (CAL). Mineral identification was attempted to use Scanning Electron Microscopy images based on the fractal geometry method and deep convolutional autoencoder networks (Karimpouli and Tahmasebi, 2019; Golsanami et al., 2021b). Calcareous cements were identified using diluted hydrochloric acid. Architectural elements refer to bodies of rock strata characterized by specific lithofacies assemblages, lithosome geometries, scales and contact relationships (Miall, 1988a, b). Lithofacies, architectural elements and sedimentary interfaces were analyzed, classified and described employing a modified version of the popular classification scheme of Miall (1988a, b). The longitudinal distribution of sedimentary stratigraphy was determined according to one or several of the following respects: weathering profile, lithology, sedimentary structure, and fossil content.

3.2. Fracture data collection

The fracture attributes include fracture strikes, dip angles, heights and spacings along scanlines that are parallel to the outcrop strike, which were systematically measured by using a geologic compass and a linen measuring tape in the outcrops (Guerriero et al., 2010). The relationships between fracture longitudinal propagation and different bounding interfaces were analyzed. The numbers of fractures terminated at and propagating through the bounding interfaces were counted, respectively. The fracture patterns in different sedimentary architecture were sketched and photographed in the field study. The fracture identification in wells of the tight sandstones of Chang 6 in Ansai Oilfield was based on cores, image logs and conventional logs using the methods proposed by Lyu et al. (2016a, 2016b) and Lai et al. (2018).

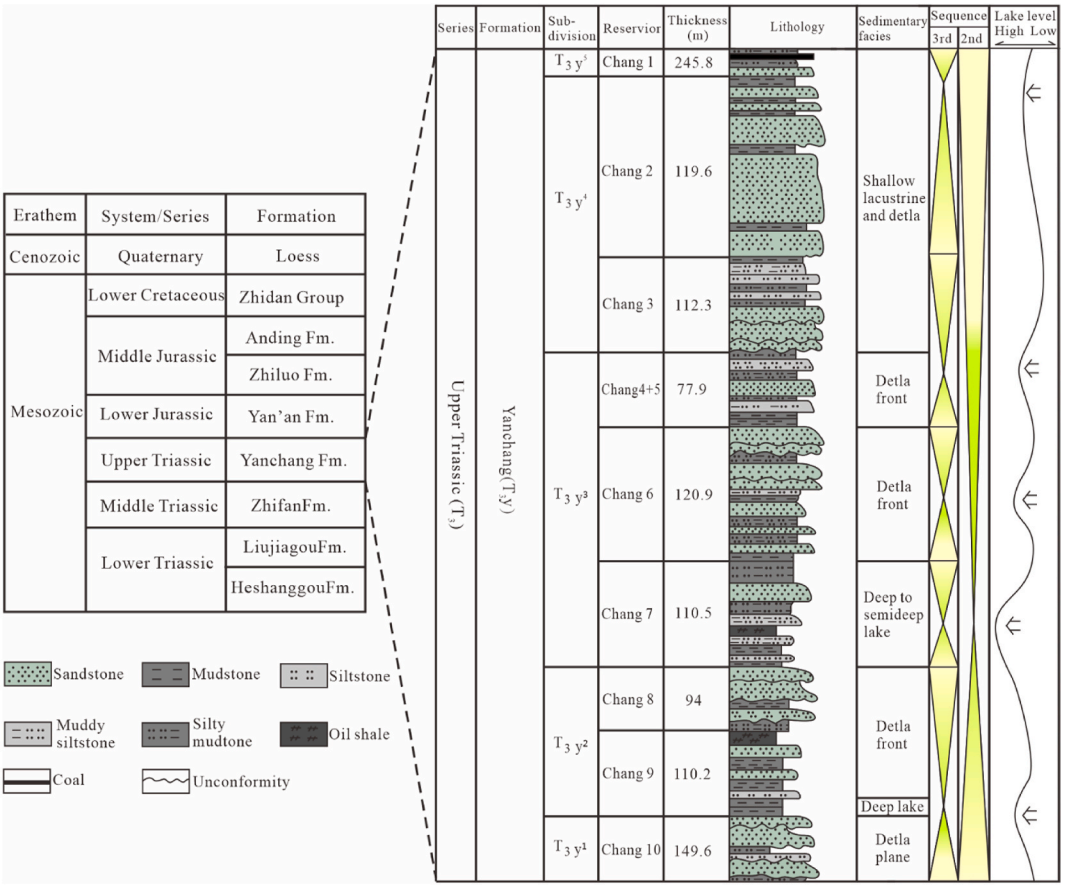

Fig. 4. Schematic stratigraphy, stratigraphic subdivision, sedimentary facies of the Yanchang Formation in the eastern part of the Ordos Basin (modified from Zhao et al., 2015; Lai et al., 2017; Qu et al., 2020).

3.3. Rock relative strength measurement

The present-day in-situ stiffness of rock was measured using an N-type Schmidt Hammer (Katz et al., 2000; Aydin and Basu, 2005) to characterize the relative competence of the present-day mechanical stratigraphy layers and rock (Ferrill and Morris, 2008; McGinnis et al., 2017). The N-type Schmidt Hammer is a portable device that measures the present-day mechanical rebound value (hereafter "rebound value R″) of a hammer impacting the rock (Ferrill and Morris, 2008). It provides a quick and inexpensive proxy for rock mechanics data since other approaches for obtaining rock mechanics data (such as Brazilian tensile test, unconfined and confined compression test, the method based on Archie's coefficients [Golsanami et al., 2020], ect.) are time consuming and expensive. The rebound analysis used in this work was followed by the approach describe by Morris et al. (2009) and Ferrill et al. (2011).

Firstly, to avoid the influence of uneven rock surface, weathering and denudation on the measured values, the rock surface, which is relatively straight and fresh, no weathering and denudation, was selected to measure. Then, the measurements were carried on subvertical rock surfaces to eliminate the gravity effect. Multiple rebound values R (at least 10 values) were measured at the same measuring point to avoid the randomness of measurement. The average value of the rebound values R was taken as the rebound value R of each measuring point. The rebound value R is a dimensionless measure of rock strength, which has been correlated to unconfined compression strength and Young's modulus through laboratory testing (Katz et al., 2000; Aydin and Basu, 2005). The rebound values R of different lithologies and the rock near where fracture terminations were obtained from Schmidt hammer in this work.

It is important to keep in mind that the measured rebound values are unlikely to reflect actual behavior of the rock when it was deforming, or even at present-day subsurface conditions. Since unloading, thermal contraction, freezing, weathering, drying, and changes in the amount, phase, or composition of fluid in the rock can all influence rock strength characteristics (Ferrill et al., 2017). However, the R-value profiles could be used to reflect some aspects of relative competence among rock layers and from locality to locality (Morris et al., 2009). The profile of relative rock mechanical property was established by the R-value profiles obtained from N-type Schmidt Hammer.

3.4. Identification of mechanical interfaces

In combination with the fracture patterns and scales, the mechanic interface was determined by the natural-fracture termination probability of the bounding interface (Underwood et al., 2003). Namely, the mechanic interface is required that the ratio of the number of the fractures terminated at the bounding interface versus the total number of fractures terminated at and propagating through the bounding interface is not less than α, which is obtained from the statistical results:

$$\frac{No.\text{ of Terminations}}{No.\text{ of Terminations}+\text{No. of Crossings}}\times 100\%\begin{cases}\geq\alpha, \text{ mechanic interface}\\ <\alpha, \text{ non}-\text{mechanic interface}\end{cases}$$

The mechanical stratigraphy in the outcrops was divided according to the longitudinal distribution of sedimentary stratigraphy, the profile of relative rock mechanical property and longitudinal distribution of mechanical interfaces. Similarly, the mechanical stratigraphy in wells was determined according to the lithology profile, the profile of relative rock mechanical property and longitudinal distribution of mechanic interfaces.

4. Results

4.1. Natural fractures

Natural fractures of the Yanchang Formation in the outcrops along Yanhe River are commonly nearly vertical to layers, and display high dip angles (Fig. 5, Supplementary Fig. 1). Four sets of natural fractures, trending east to west, northwest to southeast, north to south and northeast to southwest, are developed in the tight sandstones of Chang 6 to Chang 8. Fracture lengths are less than 14 m (45.9 ft) in most cases, and only few fracture lengths are greater than 20 m (65.6 ft) (Fig. 6a). Generally, the number of fractures decreases with the increase of fracture length. The fracture heights are generally less than 2.1 m (6.9 ft), with most of fracture heights ranging from 0.1 to 1.1 m (0.3–3.6 ft) (Fig. 6b).

4.2. The relationship between natural fractures and bounding interfaces

Field outcrop surveys have shown that fractures are usually terminated at, or propagate through, or slip along the bounding interfaces (Fig. 5; Supplementary Fig. 1).

According to the outcrops of Chang 6 to Chang 8, the relationships between natural fractures and bounding interfaces are divided to three types (Fig. 5; Supplementary Fig. 1): (1) natural fractures are developed and arrested within the layer (IF); (2) natural fractures, developed in the layer, are arrested at and perpendicular to the bounding interface (AF); (3) natural fractures penetrate through bounding interfaces, and are developed in multiple layers (TF). The first two types of fractures are intraformational fractures, and the third type of fracture is transformational fractures. About 70% of fractures are intraformational fractures, and about 30% of fractures are transformational fractures in the outcrops of Chang 6 to Chang 8 (Fig. 7).

According to the relationship between vertical fractures and layers, the patterns of vertical fractures are divided into six types (Fig. 8). (1) The first type of fracture is developed in a single layer and presents prefect bed-bounded (Fig. 8a). In this case, fractures are arrested at the bounding interfaces. Fractures developed in the same layer have the same fracture space. The greater the layer thickness, the greater space between fractures could be. (2) The second type of fracture is developed in a single layer and arrested within the layer (Fig. 8b). (3) The third type of fracture is developed in a single layer, and one tip of the fractures is arrested at the bounding interface, with another tip being arrested within the layer (Fig. 8c). (4) The fourth type of fracture is developed in multiple layers and presents prefect bed-bounded (Fig. 8d). In this case, a range of interbedded fractured layers is present. Fractures developed in the same layer have the same fracture space. With the increase number of the layers, the fracture spaces increase. (5) The fifth type of fracture cuts through multiple layers, and one tip of fractures is arrested at the bounding interface, with another tip being arrested within the layer (Fig. 8e). (6) The sixth type of fracture spans multiple layers and presents unbounded by bounding interface (Fig. 8f).

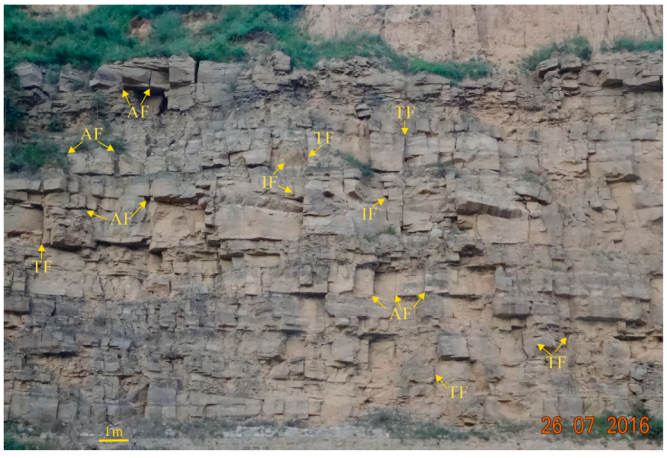

Fig. 5. Natural fractures of Chang 7 in the outcrops near Zhangjiatan Town. AF = fractures arrested at bounding interface of layers; IF = fractures arrested within the layers; TF = fractures penetrate through bounding interfaces. See Fig. 3d for the location of Zhangjiatan Town.

4.3. Bounding-interface types and their probabilities terminating fractures

According to the observation directly by naked eye, bubble indications by diluted hydrochloric acid and the Schmidt Hammer rebound values collected in each bed in the outcrops, 8 types of bounding interfaces that terminate fractures are mainly present in the study area: (1) the interface of laminae-set (Fig. 9a; Supplementary Fig. 2a) or laminae co-sets, which is corresponding to the first to the second interface (Table 1); (2) bedding surface interface (Figs. 9b and c; Supplementary Figs. 2b and 2c), which is corresponding to the second to the third interface (Table 1); (3) accretionary interface (Fig. 9c; Supplementary Fig. 2c), which is corresponding to the third interface (Table 1); (4) calcareous interbed (Fig. 9d; Supplementary Fig. 2d), which is corresponding to the second to the third interface (Table 1) mainly depended on its thickness; (5) mudstone interbed (Fig. 9e; Supplementary Fig. 2e), which is corresponding to the second to the third interface (Table 1) mainly depended on its thickness; (6) mudstone barrier (Fig. 9f; Supplementary Fig. 2f), which is corresponding to the fourth to the fifth interface (Table 1) mainly depended on its thickness; (7) calcareous barrier (Fig. 9g; Supplementary Fig. 2g), which is corresponding to the third to the fourth interface (Table 1) mainly depended on its thickness; (8) depositional scour interface (Fig. 9h; Supplementary Fig. 2h), which is corresponding to the fourth to the fifth interface (Table 1).

In combination with fracture patterns and scales, according to the statistics of the ratio of the number of fracture terminations versus the total number of fracture terminations and crossings at the 74 different bounding interfaces, the average probabilities of the calcareous barriers and the mudstone barriers terminating fractures are nearly 100% and 95.7%, respectively. The average probability of the mudstone interbed is 77%, while the average probability of the accretionary interface is 73.8%. In addition, the average probability of the depositional scour interface is 72.1%, and the average probabilities of the laminae-set interface, the bedding surface interface and the calcareous interbed are 66.7%, 25% and 15%, respectively (Table 2). According to the statistics of the 74 bounding interfaces, the probability of 11 bounding interfaces terminating fractures is less than 20%, accounting for 14.1% of the total bounding interfaces (Fig. 10). Combined with the fracture patterns at these 11 bounding interfaces, more that 80% fractures propagate through these bounding interfaces, and these bounding interfaces cannot control the fracture distribution. When the probability of the bounding interfaces terminating fractures is greater than 20%, the bounding interfaces can control the fracture distribution.

4.4. Sedimentary facies

The Chang 6 and Chang 8 in the study area are formed in a shallow water delta environment (Fu, 2013), and the sedimentary microfacies of sandstones include distributary channel (Figs. 11a, b, c, d; Supplementary Figs. 3a, b, c, d), (river) mouth bar (Fig. 11e; Supplementary Fig. 3e) and sheet sandbody (Fig. 11f; Supplementary Fig. 3f), among which the distributary channels are the dominant microfacies.

4.4.1. Distributary channel

According to the characteristics and distribution locations of distributary channels, distributary channels are mainly divided into main distributary channels (Figs. 11 a, b, c; Supplementary Figs. 3a, b, c) and terminal distributary channels (Fig. 11 d; Supplementary Fig. 3d).

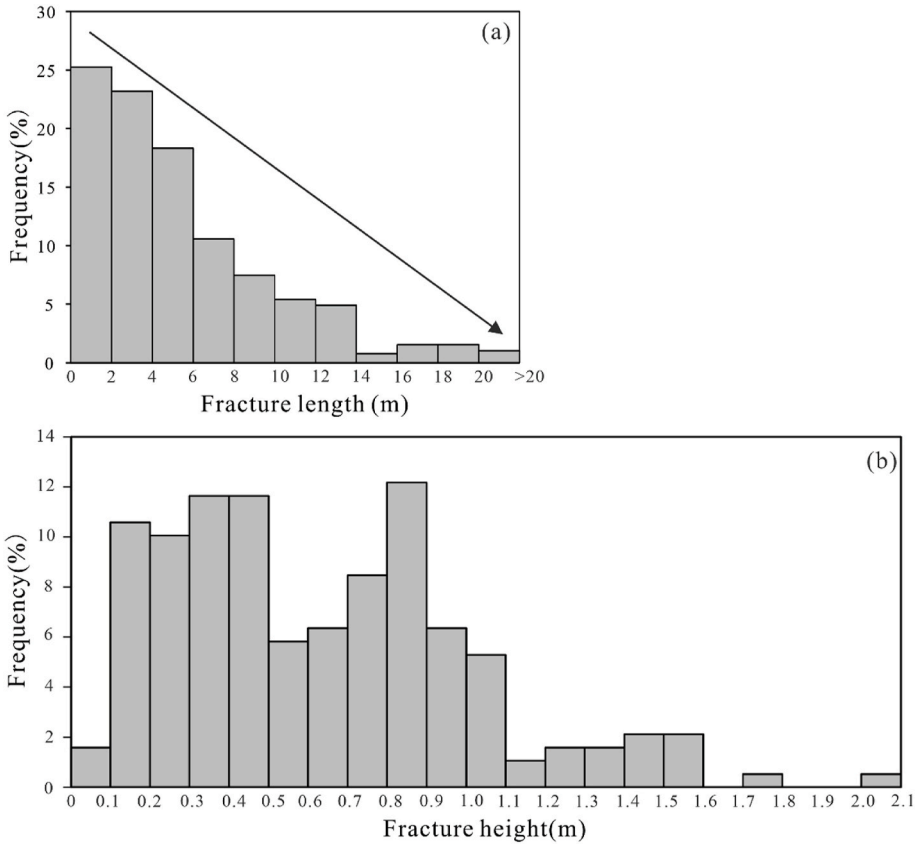

Fig. 6. (a) Fracture length distribution of Chang 6 to Chang 8 in the outcrops along Yanhe River. The number of fractures is 388. (b) Fracture height distribution of Chang 6 to Chang 8 in the outcrops along Yanhe River. The number of fractures is 189.

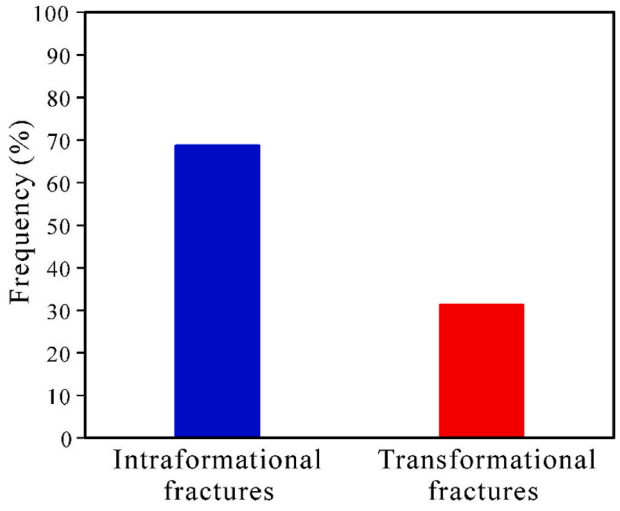

Fig. 7. The frequency distribution of intraformational and transformational fractures of Chang 6 to Chang 8 in the outcrops along Yanhe River (n = 211).

4.4.1.1. Main distributary channel. The main distributary channel is the main distributary system of shallow water delta, which is widely developed in the study area. According to the field outcrop observation, the sandbodies of the main distributary channels are formed by vertical fillings, which are mainly further divided into horizontal filling (Figs. 11a and b; Supplementary Figs. 3a and b), and arc-shaped filling (Fig. 11c; Supplementary Fig. 3c).

The sandbody is horizontally and vertically superposed in the main distributary channel with vertically horizontal filling (Figs. 11a and b; Supplementary Figs. 3a and b). It is commonly a bedding surface interface or obvious accretionary interface between each accretion. The thickness of the whole distributary channel changes little laterally. Parallel beddings are mainly developed, and cross beddings are occasionally seen in the upper part of distributary channels. The lithology is mainly fine-grained sandstone.

On the other hand, the sandbody is arc-shaped and vertically superposed in the main distributary channel with vertically arc-shaped filling (Fig. 11c; Supplementary Fig. 3c). The main distributary channel with vertical arc-shaped filling has a bedding surface interface or obvious accretionary interface between each accretion. The thickness is thick in the middle and thin to the two sides. Its lithology is mainly fine sandstone, siltstone, and muddy siltstone.

4.4.1.2. Terminal distributary channel. The terminal distributary channel develops at the end of the shallow water delta system, with weak incising (Fig. 11d; Supplementary Fig. 3d). The terminal distributary channel is wide but its thickness is small (generally less than 2 m). The thickness is relatively thick in the middle and thin in the two sides, showing the fining upward characteristics. The lithology is mainly fine sandstone and siltstone. It is commonly a bedding surface interface, whereas accretionary interface is developed in some cases.

4.4.2. Mouth bar

The sandbody of mouth bars is coarse at the top and fine at the bottom (Figs. 9c and 11e; Supplementary Figs. 2c and 3e). The lower accretion is dominated by siltstone and argillaceous siltstone, whereas the upper accretion has coarser grain size and is dominated by fine-grained sandstone. The upper and lower accretions are commonly separated by accretionary interface. Bedding surface interfaces are generally present in both upper and lower accretions. The whole

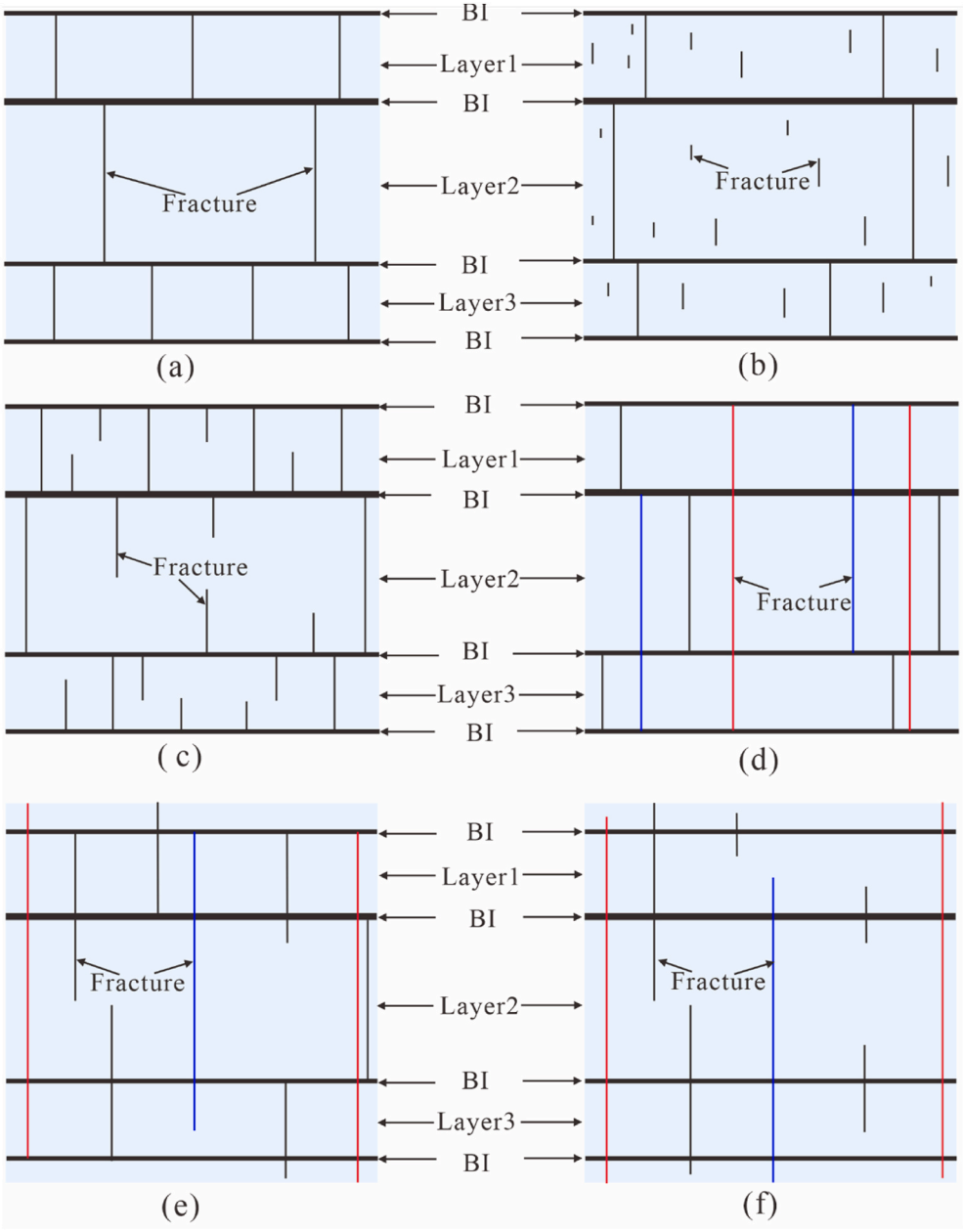

Fig. 8. Schematic diagram showing the relationship between natural fractures and bounding interfaces, BI = bounding interface: (a) fractures are developed in a single layer and present prefect bed-bounded. In this case, fractures are arrested at the bounding interfaces; (b) fractures are developed in a single layer, and arrested within the layer; (c) fractures are developed in a single layer, and one tip of the fractures is arrested at the bounding interface, with another tip being arrested within the layer; (d) fractures are developed in multiple layers and present prefect bed-bounded. In this case, a range of interbedded fractured layers is present; (e) fractures cut through multiple layers, and one tip of fractures is arrested at the bounding interface, with another tip being arrested within the layer; (f) fractures span multiple layers and are present unbounded by bounding interfaces.

sandbody of mouth bar has a lenticular shape with a flat bottom and a convex top.

4.4.3. Sheet sandbody

Sheet sandbody, with a thin thickness, is widely distributed and interbed with mudstone barriers (Fig. 11f; Supplementary Fig. 3f). It is mainly composed of siltstone, and usually has horizontal bedding or is massive.

5. Discussion

5.1. Mechanical interfaces

According to the field outcrop observations, it is possible to simultaneously observe some fractures terminating at the bounding interface and the others propagating through the bounding interface. In other words, not all bounding interfaces can constrain fracture propagation. Therefore, the above-mentioned bounding interfaces cannot be served as the mechanical interfaces controlling the distribution of all the fractures. The mechanical interfaces controlling the distribution of fractures cannot always restrain the longitudinal extension of all the fractures. Thus, it is necessary to analyze whether the bounding interface can be served as the mechanical interface for a specific area or not.

According to the probability of bounding interfaces terminating natural fractures obtained from field geological statistics, Underwood et al. (2003) defined the bounding interface that can terminate more that 50% of natural fractures as the mechanical interface in Silurian dolomite, northeastern Wisconsin. In this study, according to the statistical analysis of the average probability of 74 different bounding interfaces terminating fractures, except for calcareous interbeds (Fig. 10), the average probability of other bounding interfaces terminating fractures is more than 20%. According to the field observation, it is found that calcareous interbeds are easier to form natural fractures than non-calcareous interbeds, with few cases restricting the longitudinal propagation of fractures. In addition, different types and hierarchies of bounding interfaces have different restriction capacities for the

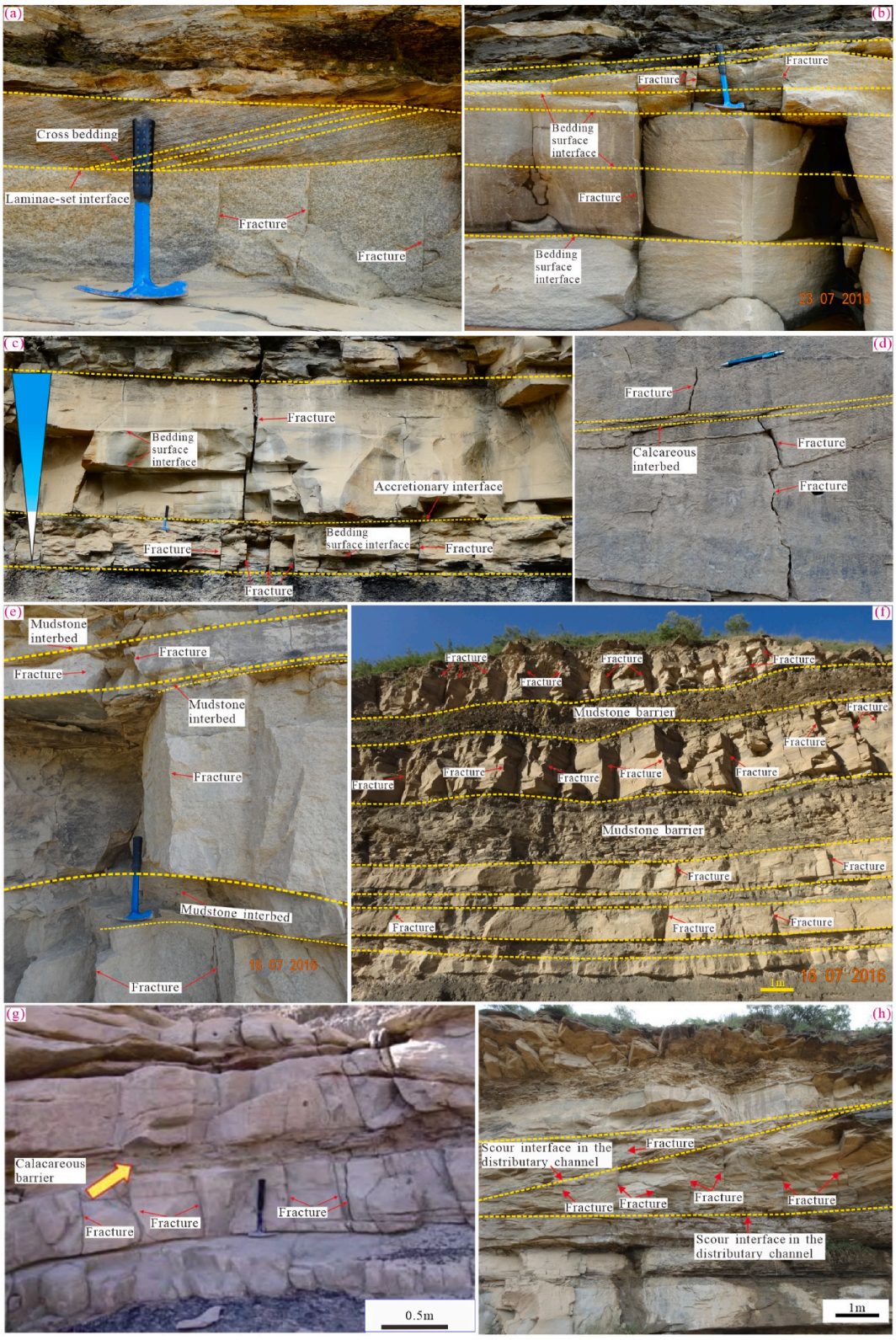

Fig. 9. Photos of bounding interfaces terminating fractures in the study area. (a) Laminae-set interface in the outcrop in Tanjiahe Village (The geological hammer stands for the size scale). (b) Bedding surface interface in the outcrop in Tanjiahe Village (The geological hammer stands for the size scale). (c) Accretionary interface and bedding surface interface in the outcrop near Zhangjiatan Town (The geological hammer stands for the size scale). (d) Calcareous interbed in the outcrop near Tanjiahe Village (The pen stands for the size scale). (e) Mudstone interbed in the outcrop near Dongjiahe Village (The geological hammer stands for the size scale). (f) Mudstone barrier in the outcrop near Wangjiahe Village. (g) Calcareous barrier in the outcrop (modified from Han et al., 2014). (h) Depositional scour interface in the distributary channel in the outcrop near Dongjiahe Village. See Fig. 3d for the locations of Dongjiahe Village, Tanjiahe Village, Zhangjiatan Town and Wangjiahe Village.

Table 1
Hierarchies of bounding interfaces in shallow water delta (modified from Miall, 1988a; Wu et al., 2013; Ahmed et al., 2014).

Reservoir architecture units	Bounding-interface hierarchies
Distributary channel-mouth bar complex	5
Distributary channel/mouth bar	4
Accretion	3
Laminae co-sets	2
Laminae set	1
Lamina	0

Table 2
The number of different bounding interfaces and their average probabilities terminating fractures.

Bounding interface types	The number of the bounding interface	The average probabilities of the bounding interface terminating fractures
Calcareous barrier	1	100%
Mudstone barrier	26	95.7%
Mudstone interbed	3	77%
Accretionary interface	8	73.8%
Depositional scour interface	11	72.1%
Laminae-set interface	1	66.7%
Bedding surface interface	23	25%
Calcareous interbed	1	15%

longitudinal propagation of fractures (Fig. 10). Thus, the bounding interface that terminates more than 20% of fractures is treated as the mechanical interface restricting fracture propagation in the tight sandstones of the study area.

5.2. Fracture hierarchy division

As previously mentioned, the different relationships between vertical fractures and layers (Fig. 8) in the tight sandstones lead to formation of fractures with different longitudinal propagations, heights and lengths. Different types and hierarchies of mechanical interfaces, even the same type of mechanical interface, have different restriction capacities for the longitudinal propagation of fractures (Fig. 10), indicating that vertical fractures have multiple scales. As mentioned above, fractures are developed in the mechanical unit and arrested at mechanical interfaces (Underwood et al., 2003; Cooke et al., 2006). According to fracture sizes and the mechanical interface which constrains fracture propagation, natural fractures generally can be divided into macro-scale, meso-scale, small-scale and micro-scale ones in the tight sandstones in the study area (Fig. 12; Supplementary Fig. 4):

Micro-scale fractures are developed with a single sandbody. Micro-scale fractures are millimeters in length or less. These fractures are commonly observed by magnification with help of microscopes, which are not easy to directly observed in the outcrops.

Small-scale fractures are also developed within a single sandbody and constrained by the mechanical interfaces, such as the interfaces of laminae set or laminae co-sets, bedding surface interfaces, accretionary interfaces, mudstone barriers, etc., and these mechanical interfaces are generally corresponding to the first to the fifth interfaces (Table 1). These fractures are mainly jointed fractures and generally normal to bedding planes. Their heights commonly vary from centimeters to decimeters.

Meso-scale fractures are developed within multiple sandbodies. These fractures are constrained by the mechanical interfaces, such as the mudstone interbeds with a certain thickness, accretionary interface, mudstone barriers, etc., which are mainly corresponding to the third to the fifth interfaces (Table 1). Meso-scale fractures cut through the interfaces of laminae set or laminae co-sets, bedding surface interface, etc., which are commonly corresponding to the first or the second interfaces (Table 1). Their heights are commonly several meters.

Macro-scale fractures are developed within sandstone groups, and constrained by the mechanical interfaces (such as the depositional scour interfaces, calcareous barriers and mudstone barriers with thick thickness), which are mainly corresponding to the fourth to the fifth interfaces (Table 1). These fractures cut through the interfaces of laminae set or laminae co-sets, mudstone interbeds and calcareous interbeds, etc., which are mainly corresponding to the first to the third interfaces (Table 1). Their heights commonly range from several to tens of meters.

According to the characteristics of multi-scale fractures, although micro-scale fractures are widely developed in the tight sandstones, multi-scale factures in the outcrops for directly observation refer to small-scale, meso-scale and macro-scale ones.

The rock mechanical properties, the thickness of mechanical stratigraphy and tectonic stress affect the longitudinal propagation and

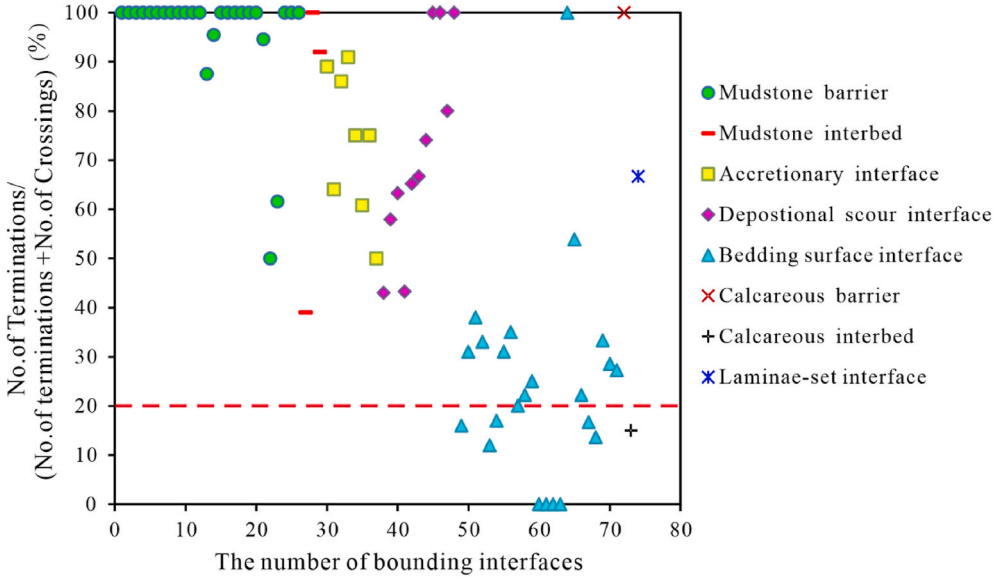

Fig. 10. The frequency distribution of natural fracture termination on different bounding interfaces.

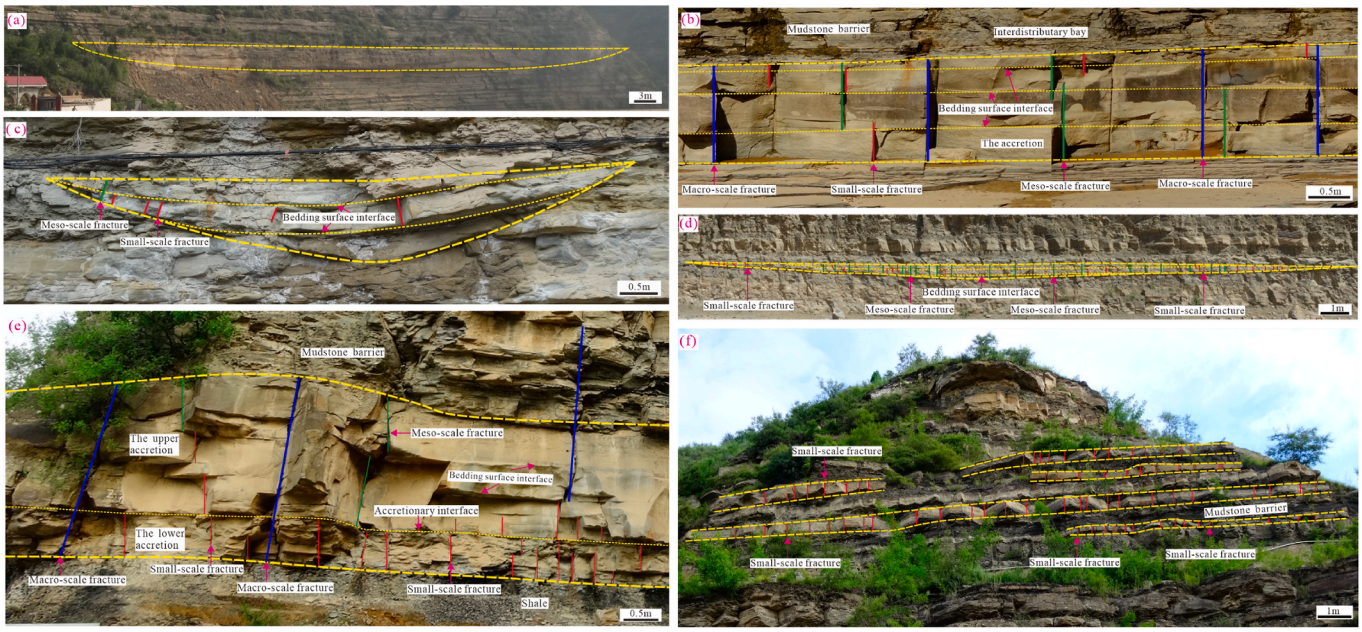

Fig. 11. Photos of main sedimentary microfacies of the tight sandstones of Chang 6 to Chang 8 in the outcrops along Yanhe River. (a) The main distributary channel with vertically horizontal fillings in the outcrop near Dongjiahe Village (the thick yellow dotted line indicates); (b) the main distributary channel with vertically horizontal fillings (the thick yellow dotted) in the outcrop in the Tanjiahe Village; (c) the main distributary channel with vertically arc-shaped fillings in the outcrop near Dongjiahe Village (the thick yellow dotted line indicates); (d) the terminal distribution channel in the outcrop in Wangjiahe Village (the thick yellow dotted line indicates); (e) the mouth bar in the outcrop near Zhangjiatan Town; (f) the sheet sand in the outcrop near Zhangjiatan Town (the thick yellow dotted lines indicate). The red lines indicate small-scale fractures, the green lines indicate meso-scale fracture and the blue lines indicate macro-scale fractures. See Fig. 3d for the locations of Dongjiahe Village, Tanjiahe Village, Zhangjiatan Town and Wangjiahe Village. (For interpretation of the references to colour in this figure legend, the reader is referred to the Web version of this article.)

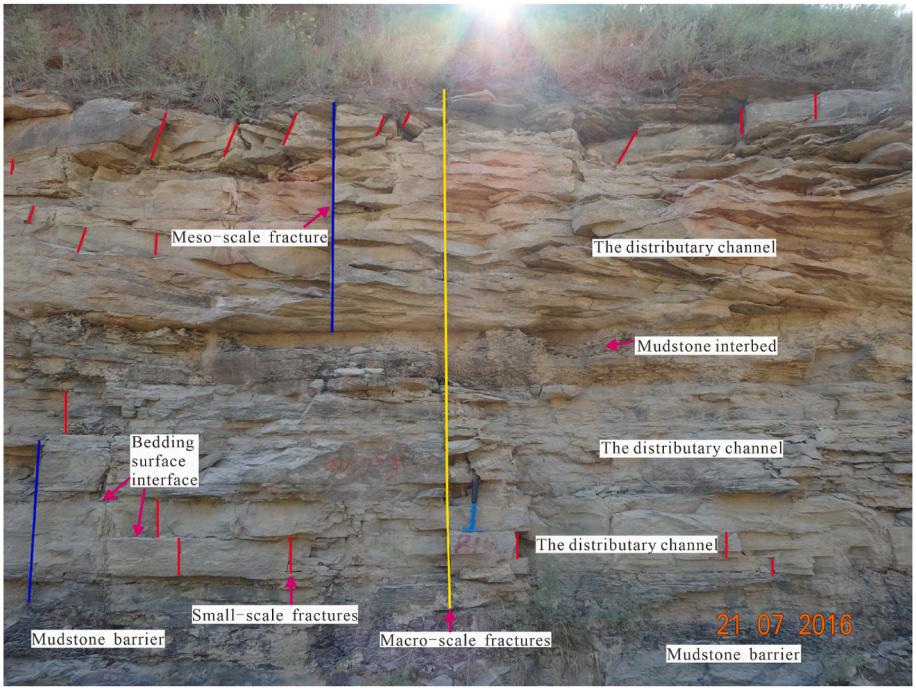

Fig. 12. Multi-scale fracture distribution of Chang 6 in the outcrop in Tanjiahe Village. See Fig. 3d for the location of Tanjiahe Village.

termination of fractures (Cooke et al., 2006; Larsen et al., 2010; Strijker et al., 2012). The restriction ability of the same type of mechanical interfaces on fracture longitudinal propagation varies in a range, namely, sometime that is strong and sometime that is weak (Fig. 10). That may attribute to the different tectonic stresses during fracture formation, the different thickness of the mechanical interfaces, and the different mechanical-property difference between mechanical interfaces and mechanical units caused by temporally changing mechanical stratigraphy. Thus, in different cases with different tectonic stresses or the different mechanical-property difference between mechanical interfaces and mechanical units, the same type of mechanical interface arresting at fractures at different scales may be different from that mentioned

previously. But the relative restriction ability of the mechanical interface arresting at fractures at different scales is determined. Namely, the restriction ability of mechanical interface arresting at macro-scale fractures is the strongest, next being that arresting at meso-scale and small-scale fractures.

5.3. Vertical fracture patterns in different sedimentary microfacies

Tectonic stress is the one of main external forces for fracture formation (Nelson et al., 2000). A sedimentary basin is usually subjected to multi-phase tectonic stresses, and the tectonic stresses usually vary in different phases (Yang, 2002). Fractures in the tight sandstones of the Yanchang Formation in the Ordos Basin are mainly formed in two periods, namely Late Jurassic and Late Cretaceous to Paleogene, which are formed due to different tectonic stress fields (Zeng et al., 2007). In addition, it is precisely that the mechanical properties of rock are changed due to diagenesis, which leads to the temporal change of mechanical stratigraphy (Shackleton et al., 2005). Consequently, the fracture pattern could be temporal change because of the temporal change of tectonic stress and mechanical stratigraphy.

According to the fracture hierarchy division, the field outcrop observation, the different restriction capacities of different mechanical interfaces and the temporally changing tectonic stress, possible vertical fracture patterns in different sedimentary microfacies could be as follows.

5.3.1. Vertical fracture patterns in the distributary channel

5.3.1.1. Vertical fracture patterns in the main distributary channel. Vertical fracture patterns in the main distributary channel with vertically horizontal fillings are mainly present three types. Firstly, when the restriction capacities of the mechanical interfaces (corresponding to the first to the third interfaces [Table 1] such as the interfaces of laminae set or laminae co-sets, the bedding surface interface and accretion interface) are strong or the tectonic stress during fracture formation is weak, the main distributary channels with vertical accretion horizontal fillings are mainly developed small-scale fractures; whereas meso-scale fractures are locally developed, and few macro-scale fractures are present (Figs. 11b and 13a; Supplementary Fig. 3b). In this case, the average space of multi-scale fractures has a positively linear correlation to the average thickness of mechanical stratigraphy (Fig. 14a). With the weaker restriction capacities of the first to the third interfaces or the greater of the tectonic stress during fracture formation, some small-scale and meso-scale fractures propagate longitudinally and cut through the first to the third interfaces to form meso-scale and macro-scale fractures, respectively. Therefore, the number of meso-scale and macro-scale fractures increase (Fig. 13b). When the restriction capacities of the first to the third interfaces are very weak or the tectonic stress during fracture formation is very great, most small-scale and meso-scale fractures propagate longitudinally and cut through the first to the third interfaces to form macro-scale fractures. Consequently, the macro-scale fractures are mainly developed, whereas small-scale and meso-scale fractures are locally developed (Fig. 13c).

Similarly, vertical fracture patterns in the main distributary channel with vertically arc-shaped fillings are mainly divided into three types. When restriction capacities of the mechanical interfaces (corresponding to the first to the third interfaces [Table 1] such as the interfaces of laminae set or laminae co-sets, bedding surface interface and accretion interface) are strong or the tectonic stress during fracture formation is weak, the main distributary channel with vertically arc-shaped fillings are mainly developed small-scale fractures, next being meso-scale fractures, whereas macro-scale fractures are locally developed (Figs. 11c and 15a; Supplementary Fig. 3c). In this case, the small-scale fractures are arrested at and vertical to the first to the third interfaces; the meso-scale fractures cut through the first to the third interfaces, and are arrested in the main distributary channel. The macro-scale fractures are mainly distributed in the two side of the main distributary channel. The macro-scale fractures penetrate the whole main distributary channel,

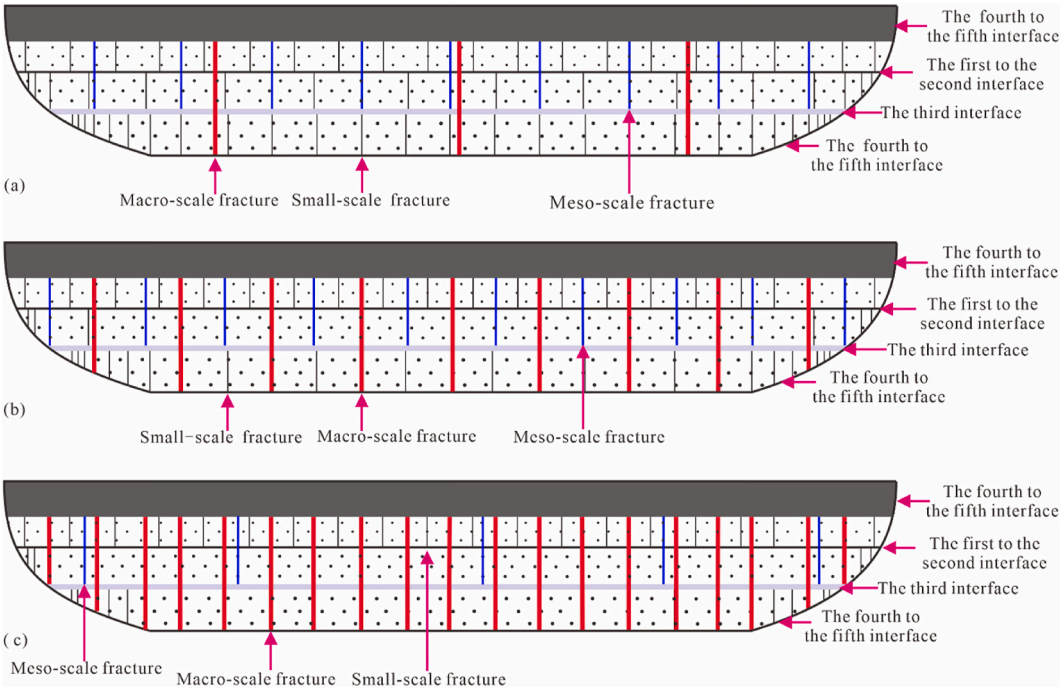

Fig. 13. The schematic diagrams showing the multi-scale fracture patterns in the distributary channel with vertically horizontal filling. (a) When restriction capacities of the mechanical interfaces (namely the first to the third interfaces such as the interfaces of laminae set or laminae co-sets, bedding surface interface and accretionary interface) are strong or the tectonic stress during fracture formation is weak; (b) with the weaker restriction capacities of the first to the third interfaces or the greater of the tectonic stress during fracture formation; (c) when the restriction capacities of the first to the third interfaces are very weak or the tectonic stress during fracture formation is very great.

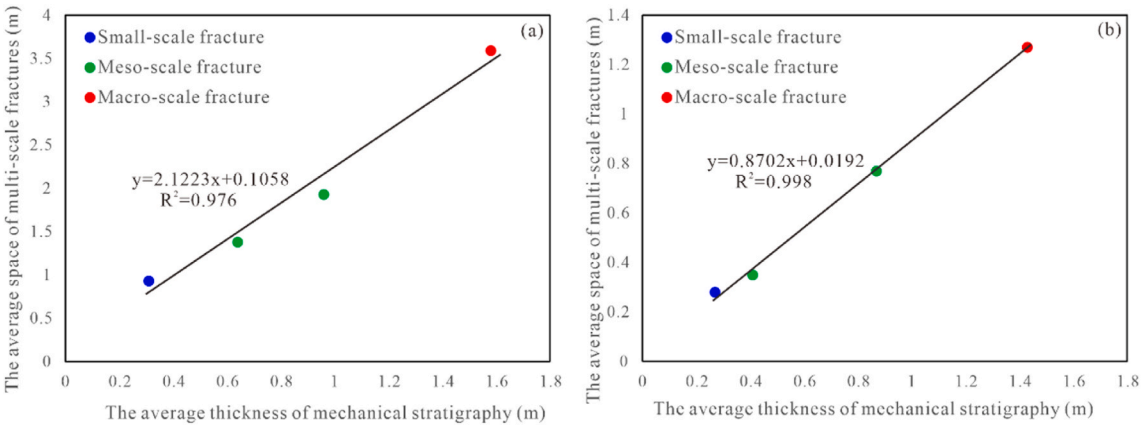

Fig. 14. The relationship between the average thickness of mechanical stratigraphy and the average space of multi-scale fractures. (a) The data were obtained from the main distributary channel with vertically horizontal filling of Chang 6 in the outcrop in Tanjiahe Village; (b) the data were obtained from the mouth bar of Chang 7 in the outcrop near Zhangjiatan Village. See Fig. 3d for the locations of Tanjiahe Village and Zhangjiatan Village.

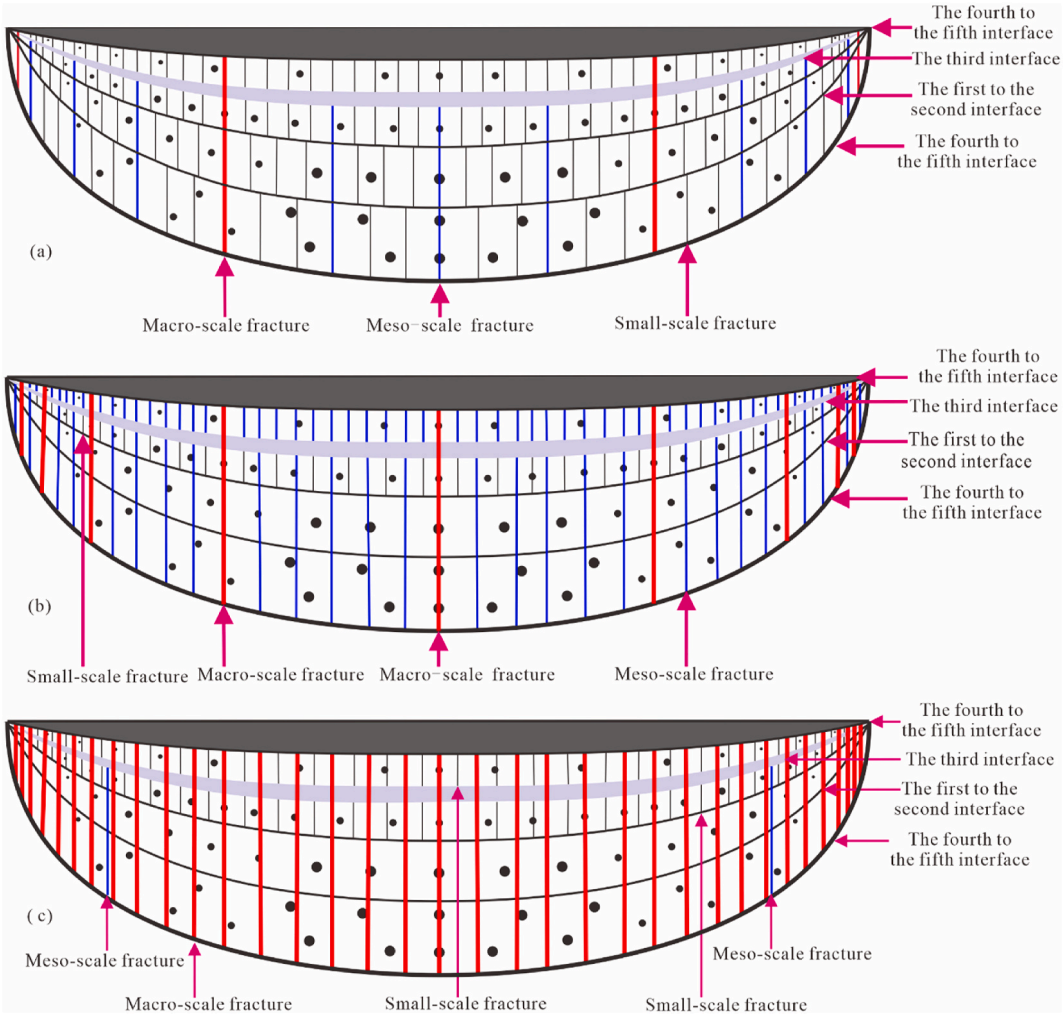

Fig. 15. The schematic diagrams showing the multi-scale fracture patterns in the distributary channel with vertically arc-shaped fillings. (a) When restriction capacities of the mechanical interfaces (namely the first to the third interfaces such as the interfaces of laminae set or laminae co-sets, bedding surface interface and accretion interface) are strong or the tectonic stress during fracture formation is weak; (b) with the weaker restriction capacities of the first to the third interfaces or the greater of the tectonic stress during fracture formation; (c) when the restriction capacities of the first to the third interfaces are very weak or the tectonic stress during fracture formation is very great.

and are arrested at the fourth to the fifth interfaces (such as mudstone barriers). The fracture space decreases from macro-scale fractures to small-scale fractures. With the weaker restriction capacities of the first to the third interfaces or the greater of the tectonic stress during fracture formation, some small-scale and meso-scale fractures propagate longitudinally and cut through the first to the third interfaces to form meso-scale and macro-scale fractures, respectively. Thus, the number of meso-scale and macro-scale fractures increase (Fig. 15b). When the restriction capacities of the first to the third interfaces are very weak or the tectonic stress during fracture formation is very great, macro-scale fractures are mainly developed, whereas small-scale and meso-scale fractures are locally developed (Fig. 15c).

5.3.1.2. Vertical fracture patterns in the terminal distributary channel. Vertical fracture patterns in the terminal distributary channels may mainly contain three types. When restriction capacities of the mechanical interfaces (the first to the third interfaces [Table 1] such as the laminae-set interface and the bedding surface interface) are strong or the tectonic stress during fracture formation is weak, the terminal distributary channels are mainly developed small-scale fractures, next being meso-scale fractures (Figs. 11d and 16a; Supplementary Fig. 3d). The spaces of fractures at the same scale in the central part of the terminal distributary channel are greater than those in the two sides of the terminal distributary channel, because the sandbody thickness decreases from the central part to the two sides of the terminal distributary channel. As the restriction ability of the first to the third interfaces becomes weak or the greater of the tectonic stress during fracture formation, some small-scale and meso-scale fractures propagate longitudinally and cut through the first to the third interfaces. Consequently, small-scale and meso-scale fractures become to be meso-scale and macro-scale fractures, respectively (Fig. 16b). When the restriction ability of the first to the third interface is very weak or the tectonic stress during fracture formation is very great, most small-scale and meso-scale fractures propagate longitudinally through the first to the third interfaces. In this case, macro-scale fractures are mainly developed in the terminal distributary channels, with few meso-scale and small-scale fractures are developed (Fig. 16c).

5.3.2. Vertical fracture patterns in the mouth bar

Vertical fracture patterns in the mouth bars may mainly present three types. The small-scale, meso-scale, and macro-scale fractures are developed in the mouth bar (Figs. 11e and 17a; Supplementary Fig. 3e). Small-scale fractures are arrested at the first to the third interfaces (Table 1) (such as the interfaces of laminae set or laminae co-sets, the bedding surface interfaces and the accretionary interfaces). Meso-scale fractures are arrested at the third interfaces, such as accretionary interfaces. Macro-scale fractures, which are distributed in the entire mouth bar, cut through the bedding surface interfaces and the accretionary interface, and arrested at the mudstone barriers (the fourth to the fifth interface). When the first to the third interfaces have strong ability to restrict the fracture longitudinal propagation or the tectonic stress during fracture formation is weak, small-scale fractures are mainly developed, next being meso-scale fractures, whereas few macro-scale fractures are developed (Figs. 11e and 17a; Supplementary Fig. 3e). In this case, the space of macro-scale fractures is the largest, next being meso-scale and small-scale fractures. The average thickness of mechanical stratigraphy and the average space of multi-scale fractures present a positively linear correlation (Fig. 14b). As the restriction ability of the first to the third interfaces becomes weaker or the tectonic stress during fracture formation becomes greater, some small-scale and meso-scale fractures propagate longitudinally and cut through the first to the third interfaces to form meso-scale and macro-scale fractures, respectively (Fig. 17b). When the restriction ability of the first to the third interfaces is very weak or the tectonic stress during fracture formation is very great, most of small-scale and meso-scale fractures propagate longitudinally to form macro-scale fractures. In this case, the mouth bar is mainly developed macro-scale fracture, whereas few small-scale and meso-scale fractures are locally developed (Fig. 17c).

5.3.3. Vertical fracture patterns in the sheet sandbody

Field outcrop observation shows that small-scale fractures are developed in the sheet sandbody and arrested at the fourth to the fifth interfaces (Table 1) such as the mudstone barriers (Figs. 11f and 18; Supplementary Fig. 3f). No meso-scale and macro-scale fractures are developed in the sheet sandbody because of the strong restriction ability of the fourth to the fifth interfaces.

5.4. Application of vertical fracture patterns for subsurface fracture prediction

Subsurface fracture prediction is important for tight oil exploration and development because fractures are major storage space and seepage channels for tight oil (Zeng and Li, 2009). Moreover high-precision fracture characterization between wells is vital for understanding subsurface fracture distribution (Lyu et al., 2016b). Though the fractures in the subsurface may be different from those in the analogous outcrops (Zeng, 2008), the vertical fracture patterns in different sedimentary facies obtained from outcrops can provide guidance for subsurface fracture characterization between wells. In addition, fracture models of different sedimentary facies could be established respectively based on the vertical fracture patterns in different sedimentary facies obtained from analog outcrops to improve the accuracy of fracture modelling.

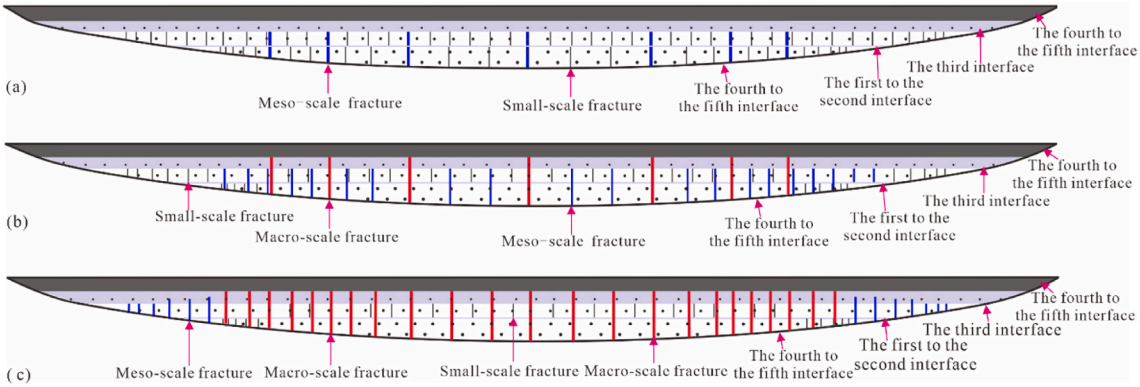

Fig. 16. The schematic diagrams showing the multi-scale fracture patterns in the terminal distributary channel. (a) When restriction capacities of the mechanical interfaces (namely the first to the third interfaces such as the laminae-set interface and bedding surface interface) are strong or the tectonic stress during fracture formation is weak; (b) with the weaker restriction capacities of the first to the third interfaces or the greater of the tectonic stress during fracture formation; (c) when the restriction capacities of the first to the third interfaces are very weak or the tectonic stress during fracture formation is very great.

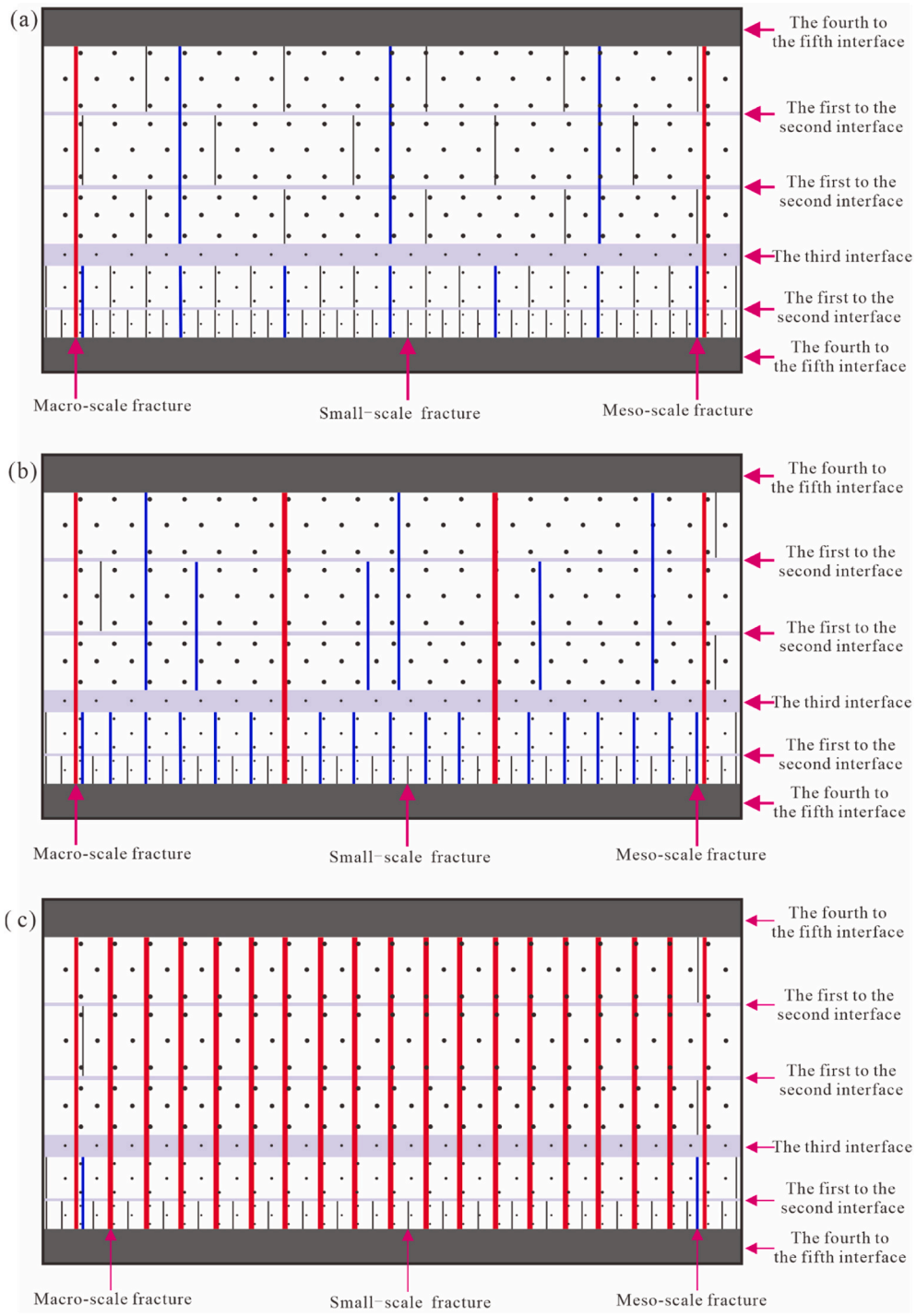

Fig. 17. The schematic diagrams showing the multi-scale fracture patterns in the mouth bar. (a) When restriction capacities of the mechanical interfaces (namely the first to the third interfaces such as the interfaces of laminae set or laminae co-sets, the bedding surface interface and accretion interface) are strong or the tectonic stress during fracture formation is weak; (b) with the weaker restriction capacities of the first to the third interfaces or the greater of the tectonic stress during fracture formation; (c) when the restriction capacities of the first to the third interfaces are very weak or the tectonic stress during fracture formation is very great.

Thus, the vertical fracture patterns in different sedimentary facies obtained from outcrops could improve the understanding of subsurface fracture distribution, which provides a geological basis for tight oil exploration and efficient development.

As mentioned above, the outcrops of Chang 6 along Yanhe River are analogous outcrops of Chang 6 in the Ansai Oilfield, which is near Yanhe river (Fig. 3b), since they have similar sedimentary and tectonic environments. Thus, the vertical fracture patterns in the distributary channels of Chang 6 obtained from the outcrops along Yanhe River could be used for the subsurface fracture pattern prediction in the tight sandstones of Chang 6 in the Ansai Oilfield.

As mentioned previously, the fracture patterns in the main distributary channel with vertically horizontal fillings of Chang 6 obtained from the outcrops along Yanhe River are established (Fig. 13a). The relationships between the space of fractures at different scales and the thickness of mechanical stratigraphy where developed corresponding fractures are unraveled (Fig. 14a). The influence of the mechanical interface such as mudstone interbed on fracture longitudinal propagation is analyzed. Then the mechanical stratigraphy in wells and fine anatomy of the internal architecture of distributary channels are determined. Finally, the fracture distribution in the main distributary channel with vertically horizontal fillings of well W1 to well W4 is predicted (Fig. 19). The results show that small-scale fractures are developed in the accretionary sandbodies, and arrested at the mudstone

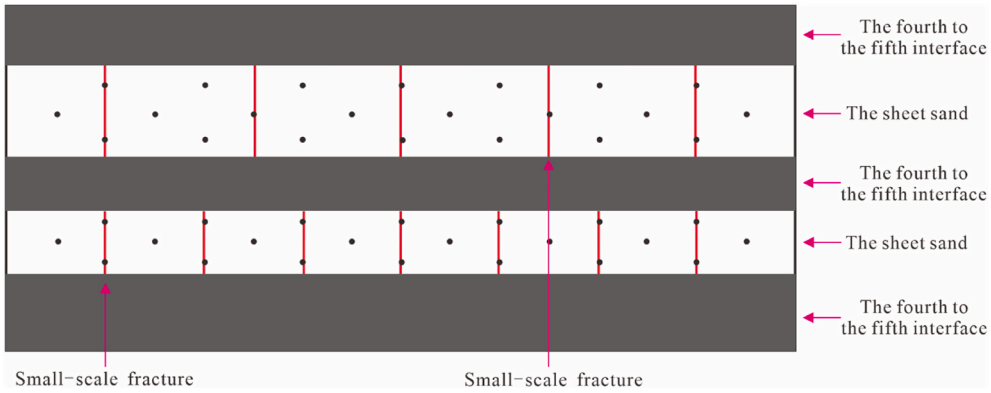

Fig. 18. The schematic diagram showing the multi-scale fracture patterns in the sheet sand. Because of the strong restriction ability of the fourth to the fifth interfaces, such as mudstone barriers, only small-scale fractures are developed in the sheet sand.

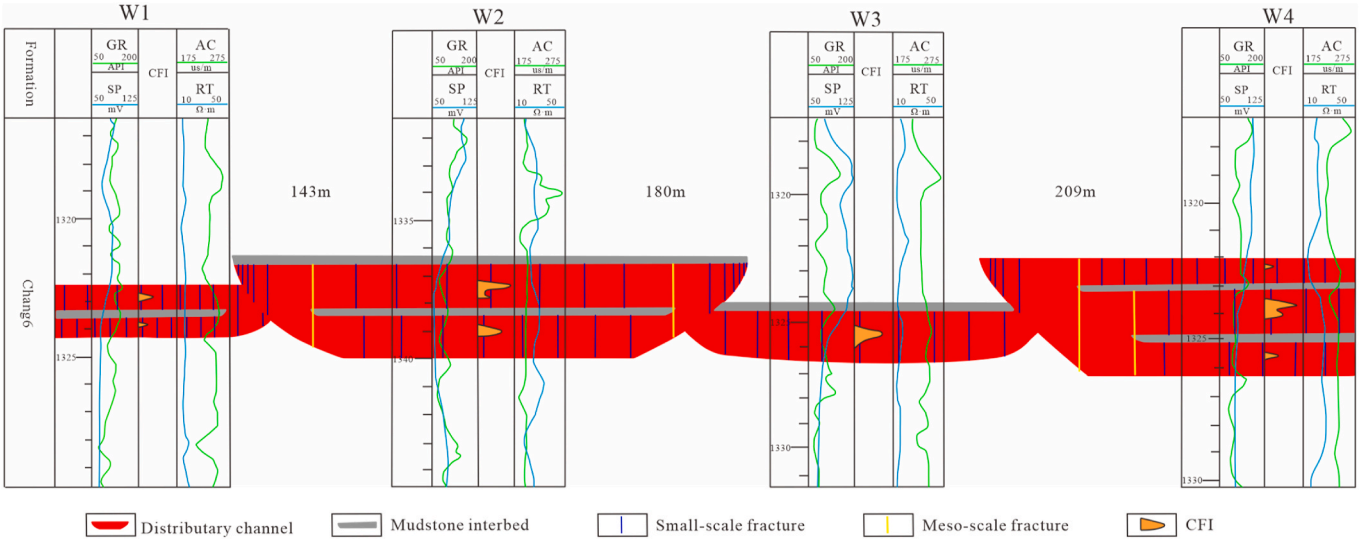

Fig. 19. Multi-scale fracture distribution in the main distributary channels among wells W1 to well W4 of Chang 6 in the Ansai Oilfeild. The predicted fractures in wells are consistent with the fractures obtained from cores and conventional logs by the method of comprehensive fracture index log (CFI) provide by Lyu et al. (2016a).

interbeds. Small-scale fracture developed in the same accretion has equal space. Meso-scale fractures are developed locally at the two side of the main distributary channels. The thickness of mudstone interbed varies from 0.2 to 0.5 m in wells W1 to W4, which has strong restriction ability arresting fracture longitudinal propagation. No fractures are present in the mudstone interbed. The predicted fractures in wells W1 and W4 are consistent with the fractures obtained from cores and conventional logs by the method of comprehensive fracture index log (CFI) provide by Lyu et al. (2016a) (Fig. 19; Lyu, 2017). Therefore, the vertical fracture pattern in different sedimentary facies obtained from outcrops could give an implication for subsurface fracture pattern prediction between wells.

6. Conclusions

(1) Seven types of mechanical interfaces are present in the Yanchang Formation of the Ordos Basin, namely, the interface of laminae-set or laminae co-sets corresponding to the first to the second interface, bedding surface interface corresponding to the second to the third interface, accretionary interface corresponding to the third interface, mudstone interbed corresponding to the second to the third interface, calcareous barrier corresponding to the third to the fourth interface, mudstone barrier and depositional scour interface both corresponding to the fourth to the fifth interface. The average probability of the mechanical interfaces terminating fractures is more than 20%.

(2) According to fracture sizes and the mechanical interfaces constraining fracture propagation, natural fractures are divided into four scales in the tight sandstones. Micro-scale fractures are developed with a single sandbody and millimeters in length or less. Small-scale fractures are also developed within a single sandbody and constrained by the first or fifth interface. Their heights commonly vary from centimeters to decimeters. Meso-scale fractures are developed within multiple sandbodies, constrained by the third to the fifth interface, and cut through the first to the second interface. Their heights are commonly several meters. Macro-scale fractures are developed within sandstone groups, constrained by the fourth to the fifth interface, and cut through the first to the third interface. Their heights are several to tens of meters.

(3) Three possible vertical fracture patterns in different sedimentary microfacies of the shallow water delta deposits are present in the study area. Generally, with increase of the restriction capacities of the mechanical interfaces terminating fractures or the decrease of tectonic stress during fracture formation, small-scale fractures are more developed, whereas meso-scale and macro-scale

fractures are less developed. The application in the tight oil sandstones of the Ansai Oilfield suggests that these vertical fracture patterns can guide subsurface fracture prediction between wells in the study area, thus providing a geological basis for tight oil exploration and efficient development.

Credit author statement

Wenya Lyu: Conceptualization, Methodology, Formal analysis, Writing - original draft, Writing - review & editing, Visualization. **Lianbo Zeng**: Supervision, Conceptualization, Writing - review & editing. **Peng Lyu**: Data curation, Resources, Investigation, Visualization. **Tao Yi**: Resources, Project administration. **Shaoqun Dong**: Resources, Investigation. **Shengjiao Wang**: Resources, Investigation. **Xiang Xu**: Resources, Investigation. **Huan Chen**: Data curation, Visualization.

Declaration of competing interest

The authors declare that they have no known competing financial interests or personal relationships that could have appeared to influence the work reported in this paper.

Acknowledgements

We thank Dr. Zhang Jiajia, Dr. Xu Zhenhua and Wang Haonan at the China University of Petroleum, Beijing for their constructive help. This work is financially support by National Natural Science Foundation of China (No. 42002135), the Strategic Cooperation Technology Projects of CNPC and CUPB (No. ZLZX2020-02), and Science Foundation of China University of Petroleum, Beijing (No.2462017YJRC057). We thank the Editors of Journal of Petroleum Science and Engineering for their diligent efforts in improving our manuscript, and two reviewers are acknowledged for their constructive comments.

Appendix A. Supplementary data

Supplementary data to this article can be found online at https://doi.org/10.1016/j.petrol.2022.110247.

References

Ahmed, S., Bhattacharya, J.P., Garza, D.E., Li, Y.Y., 2014. Facies Architecture and Stratigraphic Evolution of A River-Dominated Delta Front, Turonian Ferron Sandstone, Utah, U.S.A. J. Sediment. Res. 84, 97–121.

Aydin, A., Basu, A., 2005. The Schmidt hammer in rock material characterization. Eng. Geol. 81 (1), 1–14.

Balsamo, F., Bezerra, F.H.R., Klimchouk, A.B., Cazarin, C.L., Auler, A.S., Nogueira, F.C., 2020. Influence of fracture stratigraphy on hypogene cave development and fluid flow anisotropy in layered carbonates, NE Brazil. Mar. Petrol. Geol. 114 (104507), 1–14.

Barbier, M., Hamon, Y., Callot, J.P., Floquet, M., Daniel, J.M., 2012. Sedimentary and diagenetic controls on the multiscale fracturing pattern of a carbonate reservoir: The Madison Formation (Sheep Mountain, Wyoming, USA). Mar. Petrol. Geol. 29, 50–67.

Boersma, Q.D., Douma, L.A.N.R., Bertotti, G., Barnhoorn, A., 2020. Mechanical controls on horizontal stresses and fracture behaviour in layered rocks: A numerical sensitivity analysis. J. Struct. Geol. 130, 1–13.

Cawood, A.J., Bond, C.E., 2018. 3D mechanical stratigraphy of a deformed multi-layer: Linking sedimentary architecture and strain partitioning. J. Struct. Geol. 106, 54–69.

Chen, S.Q., Zeng, L.B., Huang, P., Sun, S.H., Zhang, W.L., Li, X.Y., 2016. The application study on the multiscale integrated prediction method to fractured reservoir description. Appl. Geophys. 13 (1), 80–92.

Cooke, M.L., Simo, J.A., Underwood, C.A., Rijken, P., 2006. Mechanical stratigraphic controls on fracture patterns within carbonates and implications for groundwater flow. Sediment. Geol. 184 (3), 225–239.

Dashti, R., Rahimpour-Bonab, H., Zeinali, M., 2018. Fracture and mechanical stratigraphy in naturally fractured carbonate reservoirs-A case study from Zagros region. Mar. Petrol. Geol. 97, 466–479.

Du, S.H., Shi, Y.M., Guan, P., 2019. Fluid filling rule in intra-granular pores of feldspar and fractal characteristics: A case study on Yanchang Formation tight sandstone reservoir in Ordos Basin. Earth Sci. 44 (12), 4252–4263. https://doi.org/10.3799/dqkx.2018.199 (In Chinese with English abstract).

Eia, 2021. Petroleum and other liquids. In: Annual Energy Outlook 2021. https://www.eia.gov/outlooks/aeo/pdf/02%20AEO2021%20Petroleum.pdf.

Ferrill, D.A., Morris, A.P., 2008. Fault zone deformation controlled by carbonate mechanical stratigraphy, Balcones fault system, Texas. AAPG Bull. 92 (3), 359–380.

Ferrill, D.A., Morris, A.P., McGinnis, R.N., Smart, K.J., Ward, W.C., 2011. Fault zone deformation and displacement partitioning in mechanically layered carbonates: The Hidden Valley fault, central Texas. AAPG Bull. 95 (8), 1383–1397.

Ferrill, D.A., Morris, A.P., McGinnis, R.N., Smart, K.J., Wigginton, S.S., Hill, N.J., 2017. Mechanical stratigraphy and normal faulting. J. Struct. Geol. 94, 275–302.

Fu, J., 2013. Research on Reservoir Architecture and Quality Difference of Shallow-Water Delta: a Case Study of the Yanchang Formation in Ordos Basin. Doctoral thesis. China University of petroleum, Beijing, p. 127 (in Chinese with English abstract).

Giuffrida, A., Agosta, F., Rustichelli, A., Panza, E., La Bruna, V., Eriksson, E., Torrieri, S., Giorgioni, M., 2020. Fracture stratigraphy and DFN modelling of tight carbonates, the case study of the Lower Cretaceous carbonates exposed at the Monte Alpi (Basilicata, Italy). Mar. Petrol. Geol. 112 (104045), 1–20.

Golsanami, N., Bakhshi, E., Yan, W.C., Dong, H.M., Barzgar, E., Zhang, G.C., Mahbaz, S., 2020. Relationships between the geomechanical parameters and Archie's coefficients of fractured carbonate reservoirs: a new insight. Energy Sources, Part A Recovery, Util. Environ. Eff. 1–25.

Golsanami, N., Zhang, X., Yan, W., Yu, L., Dong, H., Dong, X., Cui, L., Jayasuriya, M.N., Fernando, S.G., Barzgar, E., 2021a. NMR-Based Study of the Pore Types' Contribution to the Elastic Response of the Reservoir Rock. Energies 14 (1513), 1–26.

Golsanami, N., Fernando, S.G., Jayasuriya, M.N., Yan, W.C., Dong, H.M., Cui, L.K., Dong, X., Barzgar, E., 2021b. Fractal Properties of Various Clay Minerals Obtained from SEM Images. Geofluids 5516444, 1–18.

Guerriero, V., Iannace, A., Mazzoli, S., Parente, M., Vitale, S., Giorgioni, M., 2010. Quantifying uncertainties in multi-scale studies of fractured reservoir analogues: Implemented statistical analysis of scan line data from carbonate rocks. J. Struct. Geol. 32 (9), 1271–1278. https://doi.org/10.1016/j.jsg.2009.04.016.

Han, R.B., Liu, Q., Jiang, T.W., Xu, H.M., Xu, Z.H., Zhao, L., Lei, C., Zhang, P.C., 2014. Feature, origin and distribution of calcareous interlayers: A case of Carboniferous Donghe sandstone in Hade Oil Field, Tarim Basin, NW China. Petrol. Explor. Dev. 41 (4), 428–437, 413(in Chinese with English abstract).

He, Z.X., Yang, H., Yuan, X.Q., 2004. Atlas of Geological Outcrops of the Ordos Basin (In Chinese). Petroleum Industry Press, Beijing, p. 422 (in Chinese).

He, J., Feng, S.B., Yuan, X.Q., Han, P., Xie, G.W., Zhang, C.L., 2011. Sandstone component of outcrops of Yanchang Formation in the margin of Ordos Basin and its geological significance. Lithol. Reserv. 23 (6), 30–36, 43 (In Chinese with English abstract).

Ju, W., Hou, G.T., Feng, S.B., Zhao, W.T., Zhang, J.Z., You, Y., Zhan, Y., Yu, X., 2014. Quantitative prediction of the Yanchang Formation Chang 6, reservoir tectonic fracture in the Qingcheng-Heshui Area, Ordos Basin. Earth Sci. Front. 21 (6), 310–320 (in Chinese with English abstract).

Karimpouli, S., Tahmasebi, P., 2019. Segmentation of digital rock images using deep convolutional autoencoder networks. Comput. Geosci. 126, 142–150.

Katz, O., Reches, Z., Roegiers, J.C., 2000. Evaluation of mechanical rock properties using a Schmidt Hammer. Int. J. Rock Mech. Min. Sci. 37 (4), 723–728.

Lai, J., Wang, G.W., Ran, Y., Zhou, Z.L., Cui, Y.F., 2016. Impact of diagenesis on the reservoir quality of tight oil sandstones: The case of upper Triassic Yanchang Formation Chang 7 oil layers in Ordos Basin, China. J. Petrol. Sci. Eng. 14, 54–65.

Lai, J., Wang, G.W., Chen, J., Wang, S.C., Zhou, Z.L., Fan, X.Q., 2017. Origin and distribution of carbonate cement in tight sandstones: the upper Triassic Yanchang Formation Chang 8 oil layer in west Ordos Basin, China. Geofluids 2017, 1–13.

Lai, J., Wang, G.W., Wang, S., Cao, J.T., Li, M., Pang, X.J., Han, C., Fan, X.Q., Yang, L., He, Z.B., Qin, Z.Q., 2018. A review on the applications of image logs in structural analysis and sedimentary characterization. Mar. Petrol. Geol. 95, 139–166.

Lai, J., Wang, S., Wang, G.W., Shi, Y.J., Zhao, T.P., Pang, X.J., Fan, X.C., Qin, Z.Q., Fan, X.Q., 2019. Pore structure and fractal characteristics of Ordovician Majiagou carbonate reservoirs in Ordos Basin, China. AAPG (Am. Assoc. Pet. Geol.) Bull. 103 (11), 2573–2596.

Lamarche, J., Lavenu, A.P.C., Gauthier, B.D.M., Guglielmi, Y., Jayet, O., 2012. Relationships between fracture patterns, geodynamics and mechanical stratigraphy in Carbonates (South-East Basin, France). Tectonophysics 581, 231–245.

Larsen, B., Gudmundsson, A., Grunnaleite, I., Sælen, G., Talbot, M.R., Buckley, S.J., 2010. Effects of sedimentary interfaces on fracture pattern, linkage, and cluster formation in peritidal carbonate rocks. Mar. Petrol. Geol. 27 (7), 1531–1550.

Laubach, S.E., Olson, J.E., Gross, M.R., 2009. Mechanical and fracture stratigraphy. AAPG (Am. Assoc. Pet. Geol.) Bull. 93 (11), 1413–1426.

Li, D.L., Shi, Q.M., Mi, N.Z., Xu, Y., Wang, X.K., Tao, W.X., 2020. The type, origin and preservation of organic matter of the fine-grain sediments in Triassic Yanhe Profile, Ordos Basin, and their relation to paleoenvironment condition. J. Petrol. Sci. Eng. 188, 1–14.

Lyu, P., 2017. Research on Fracture Distribution Pattern Based on the Internal Architectures of Distributary Channels. Master's Thesis. China University of Petroleum, Beijing, p. 98 (in Chinese with English abstract).

Lyu, W.Y., Zeng, L.B., Liu, Z.Q., Liu, G.P., Zu, K.W., 2016a. Fracture responses of conventional logs in tight-oil sandstones: A case study of the upper Triassic Yanchang Formation in southwest Ordos Basin, China. AAPG (Am. Assoc. Pet. Geol.) Bull. 100 (9), 1399–1417.

Lyu, W.Y., Zeng, L.B., Liu, J., Wang, C.Y., Zhu, J., 2016b. Fracture research progress in low permeability tight reservoirs. Geol. Sci. Technol. Inf. 35 (4), 66–75 (in Chinese with English abstract).

Lyu, W.Y., Zeng, L.B., Liao, Z.H., Ji, Y.Y., Lyu, P., Dong, S.Q., 2017. Fault damage zone characterization in tight-oil sandstones of the Upper Triassic Yanchang Formation in

the southwest Ordos Basin, China: Integrating cores, image logs, and conventional logs. Interpretation 5 (4), P27–SP39. https://doi.org/10.1190/INT-2016-0231.1.
Lyu, W.Y., Zeng, L.B., Zhou, S.B., Du, X.S., Xia, D.L., Liu, G.P., Li, J., Weng, J.Q., 2019. Natural fractures in tight-oil sandstones: A case study of the upper Triassic Yanchang Formation in the southwestern Ordos Basin. China. AAPG (Am. Assoc. Pet. Geol.) Bull. 103 (10), 2343–2367.
Lyu, W.Y., Zeng, L.B., Chen, S.Q., Lyu, P., Dong, S.Q., Hui, C., Li, R.Q., Wang, H.N., 2021. Characterization methods of multi-scale natural fractures in tight and low-permeability sandstone reservoirs. Geol. Rev. 67 (2), 543–556 (in Chinese with English abstract).
McGinnis, R.N., Ferrill, D.A., Morris, A.P., Smart, K.J., Lehrmann, D., 2017. Mechanical stratigraphic controls on natural fracture spacing and penetration. J. Struct. Geol. 95, 160–170.
Miall, A.D., 1988a. Architectural elements and bounding surfaces in fluvial deposits, anatomy of the Kayenta Formation (Lower Jurassic), southwest Colorado. Sediment. Geol. 55 (3), 233–262.
Miall, A.D., 1988b. Reservoir heterogeneities in fluvial sandstone: lessons from outcrop studies. Am. Assoc. Petrol. Geol. Bull. 72 (6), 682–e697.
Morris, A.P., Ferrill, D.A., McGinnis, R.N., 2009. Mechanical stratigraphy and faulting in Cretaceous carbonates. AAPG Bull. 93 (11), 1459–1470.
Nelson, R.A., Moldovanyi, E.P., Matcek, C.C., Azpiritxaga, I., Bueno, E., 2000. Production characteristics of the fractured reservoirs of the La Paz field. Maracaibo Basin, Venezuela: AAPG (Am. Assoc. Pet. Geol.) Bull. 84 (11), 1791–1809. https://doi.org/10.1306/8626C393-173B-11D7-8645000102C1865D.
Ogata, K., Storti, F., Balsamo, F., Tinterri, R., Bedogni, E., Fetter, M., Gomes, L., Hatushika, R., 2017. Sedimentary facies control on mechanical and fracture stratigraphy in turbidites. GSA Bullet. 129 (20), 76–92.
Panza, E., Agosta, F., Rustichelli, A., Zambrano, M., Tondi, E., Prosser, G., Giorgioni, M., Janiseck, J.M., 2016. Fracture stratigraphy and fluid flow properties of shallow-water, tight carbonates: The case study of the Murge Plateau (southern Italy). Mar. Petrol. Geol. 73, 350–370.
Qu, H.J., Yang, B., Gao, S.L., Zhao, J.F., Han, X., Chen, S., Hayat, K., 2020. Controls on hydrocarbon accumulation by facies and fluid potential in large-scale lacustrine petroliferous basins in compressional settings: A case study of the Mesozoic Ordos Basin, China. Mar. Petrol. Geol. 122, 1–18.
Rustichelli, A., Tondi, E., Agosta, F., Cilona, A., Giorgioni, M., 2012. Development and distribution of bed-parallel compaction bands and pressure solution seams in carbonates (Bolognano Formation, Majella Mountain, Italy). J. Struct. Geol. 37, 181–199.
Rustichelli, A., Agosta, F., Tondi, E., Spina, V., 2013. Spacing and distribution of bed-perpendicular joints throughout layered, shallow-marine carbonates (Granada Basin, southern Spain). Tectonophysics 582, 188–204.
Shackleton, J.R., Cooke, M.L., Sussman, A.J., 2005. Evidence for temporally changing mechanical stratigraphy and effects on joint-network architecture. Geology 33 (2), 101–104.
Strijker, G., Bertotti, G., Luthi, S.M., 2012. Multi-scale fracture network analysis from an outcrop analogue: A case study from the Cambro-Ordovician clastic succession in Petra, Jordan. Mar. Petrol. Geol. 38 (1), 104–116.
Underwood, C.A., Cooke, M.L., Simo, J.A., Muldoon, M.A., 2003. Stratigraphic controls on vertical fracture patterns in Silurian dolomite, northeastern Wisconsin. AAPG (Am. Assoc. Pet. Geol.) Bull. 87 (1), 121–142.
Wang, B.L., Zhou, W., Deng, H.C., Liu, Y., Lei, T., Fan, L.L., 2013. Quantitative evaluation of fracture distribution of Chang-9 Member in Honghe Oilfield, Ordos Basin. Xinjing Pet. Geol. 34 (6), 653–656 (in Chinese with English abstract).
Wu, S.H., Ji, Y.L., Yue, D.L., Yin, S.L., 2013. Discussion on hierarchical scheme of architectural units in clastic deposits. Geol. J. China Univ. 19 (1), 12–22 (in Chinese with English abstract).
Xu, X.Y., Wang, W.F., 2020. The recognition of potential fault zone in Ordos Basin and its reservoir control. Earth Sci. 45 (5), 1754–1768. https://doi.org/10.3799/dqkx.2019.175 (In Chinese with English abstract).
Yang, J.J., 2002. Tectonic Evolution and Hydrocarbon Distribution in Ordos Basin. Petroleum Industry Press, Beijing, p. 228 (in Chinese).
Yang, S.B., Geng, X.X., Guo, Q.Y., Hou, G.T., Liu, Z.B., 2008. Mesozoic tectonic evolution in north section of the western margin of Ordos Basin. Geol. Rev. 54 (3), 307–315 (in Chinese with English abstract).
Yang, H., Li, S.X., Liu, X.Y., 2013. Characteristics and resource prospects of tight oil and shale oil in Ordos Basin. Acta Pet. Sin. 34 (1), 1–11. https://doi.org/10.7623/syxb201301001 (in Chinese with English abstract).
Zeng, L.B., Li, Z.X., Shi, C.G., Wan, Z.G., Zhao, J.Y., Wang, Y.K., 2007. Characteristics and origin of fractures in the extra low-permeability sandstone reservoirs of the upper Triassic Yanchang Formation in the Ordos Basin. Acta Geol. Sin. 81 (2), 174–180 (in Chinese with English abstract).
Zeng, L.B., 2008. Formation and Distribution of Fractures in Low Permeability Sandstone Reservoir. Science Press, Beijing, p. 169 (in Chinese).
Zeng, L.B., Li, X.Y., 2009. Fractures in sandstone reservoirs with ultra-low permeability: A case study of the Upper Triassic Yanchang Formation in the Ordos Basin, China. AAPG (Am. Assoc. Pet. Geol.) Bull. 93 (4), 461–477.
Zeng, L.B., Su, H., Tang, X.M., Peng, Y.M., Gong, L., 2013. Fractured tight sandstone oil and gas reservoirs: A new play type in the Dongpu depression. Bohai Bay Basin, China: AAPG (Am. Assoc. Pet. Geol.) Bull. 97 (3), 363–377. https://doi.org/10.1306/09121212057.
Zhang, H., 1996. Mesozoic and Cenozoic paleotectonic-stress field of Ordos Basin. J. Geol. Miner. Resour. North China 11 (1), 87–92 (in Chinese with English abstract).
Zhang, M.Z., Ji, L.M., Wu, Y.D., He, C., 2015. Palynofacies and geochemical analysis of the Triassic Yanchang Formation, Ordos Basin: Implications for hydrocarbon generation potential and the paleoenvironment of continental source rocks. Int. J. Coal Geol. 152 (12), 159–176.
Zhao, J.F., Mountney, N.P., Liu, C.Y., Qu, H.J., Lin, J.Y., 2015. Outcrop architecture of a fluvio-lacustrine succession: upper Triassic Yanchang Formation, Ordos Basin, China. Mar. Petrol. Geol. 68, 394–413.
Zhou, X.G., Zhang, L.Y., Huang, C.J., Wan, X.L., 2012. Distraction network conceptual model and validity of fractures in Chang 63 low permeable reservoir in Huaqing Area. J. Jilin Univ. (Earth Sci. Ed.) 42 (3), 689–697 (in Chinese with English abstract).
Zou, C.N., Zhu, R.K., Bai, B., Yang, Z., Hou, L.H., Zha, M., Fu, J.H., Shao, Y., Liu, K.Y., Cao, H., Yuan, X.J., Tao, S.Z., Tang, X.M., Wang, L., Li, T.T., 2015. Significance, geologic characteristics, resource potential and future challenges of tight oil and shale oil. Bull. China Soc. Mineral Petrol. Geochem. 34 (1), 3–17 (In Chinese with English abstract).